Ena/VASP regulates mDia2-initiated filopodial length, dynamics, and function

Melanie Barzik[a,*], Leslie M. McClain[a], Stephanie L. Gupton[b], and Frank B. Gertler[a]
[a]David H. Koch Institute for Integrative Cancer Research, Massachusetts Institute of Technology, Cambridge, MA 02139; [b]Department of Cell Biology and Physiology, University of North Carolina at Chapel Hill, Chapel Hill, NC 27599

ABSTRACT **Filopodia are long plasma membrane extensions involved in the formation of adhesive, contractile, and protrusive actin-based structures in spreading and migrating cells. Whether filopodia formed by different molecular mechanisms equally support these cellular functions is unresolved. We used Enabled/vasodilator-stimulated phosphoprotein (Ena/VASP)–deficient MV^{D7} fibroblasts, which are also devoid of endogenous mDia2, as a model system to investigate how these different actin regulatory proteins affect filopodia morphology and dynamics independently of one another. Filopodia initiated by either Ena/VASP or mDia2 contained similar molecular inventory but differed significantly in parameters such as number, length, F-actin organization, lifetime, and protrusive persistence. Moreover, in the absence of Ena/VASP, filopodia generated by mDia2 did not support initiation of integrin-dependent signaling cascades required for adhesion and subsequent lamellipodial extension, thereby causing a defect in early cell spreading. Coexpression of VASP with constitutively active mDia2$^{M/A}$ rescued these early adhesion defects. We conclude that Ena/VASP and mDia2 support the formation of filopodia with significantly distinct properties and that Ena/VASP regulates mDia2-initiated filopodial morphology, dynamics, and function.**

Monitoring Editor
Mark H. Ginsberg
University of California, San Diego

Received: Feb 5, 2014
Revised: Jun 6, 2014
Accepted: Jun 24, 2014

INTRODUCTION

Cell migration requires the coordination of a variety of processes such as substrate sensing, dynamic remodeling of cell–substrate adhesions, and generation of contractile forces and protrusive structures (Lauffenburger and Horwitz, 1996; Small *et al.*, 2002; Parsons *et al.*, 2010). Regulated actin polymerization at the leading edge drives the protrusion of veil-like lamellipodia and thin, finger-like filopodia (Small *et al.*, 2002). Lamellipodia contain a meshwork of short, branched actin filaments nucleated by the Arp2/3 complex and provide the driving force required for cell motility and migration. Filopodia are composed of long, unbranched and tightly cross-linked parallel actin filaments that are oriented with their fast-growing barbed ends toward the filopodium tip (Pollard and Borisy, 2003; Chhabra and Higgs, 2007). During cell migration, filopodia probe the environment for guidance cues, serve as "sticky fingers" to promote the initial attachment to the substrate, and trigger signal transduction cascades to regulate the formation and maturation of stable focal adhesions (Davenport *et al.*, 1993; Partridge and Marcantonio, 2006; Galbraith *et al.*, 2007; Schäfer *et al.*, 2010).

Whereas the individual key regulators that control the actin cytoskeleton architecture are well studied, it is unclear how cells orchestrate an assortment of different actin regulatory proteins to fine tune the spatiotemporal formation of actin protrusions. In particular, it is unclear how proteins with seemingly similar functions can produce structurally and functionally distinct protrusions and how individual components within the system of actin regulators are interconnected to promote coordinated actin dynamics and protrusions. We sought to explore these open questions by investigating filopodia assembly downstream of two F-actin polymerases, mammalian Diaphanous 2 (mDia2) and vasodilator-stimulated phosphoprotein (VASP).

Proteins of the Enabled (Ena)/VASP family (mammalian Ena [Mena], EVL, and VASP in vertebrates; Ena in *Drosophila*) promote

This article was published online ahead of print in MBoC in Press (http://www.molbiolcell.org/cgi/doi/10.1091/mbc.E14-02-0712) on July 2, 2014.

*Present address: Laboratory of Molecular Genetics, National Institute on Deafness and Other Communication Disorders, National Institutes of Health, Bethesda, MD 20892.

Address correspondence to: Melanie Barzik (melanie.barzik@nih.gov).

Abbreviations used: CP, capping protein; DRF, Diaphanous-related formin; ECM, extracellular matrix; Ena/VASP, Enabled/vasodilator-stimulated phosphoprotein; EVH, Ena/VASP homology; FAK, focal adhesion kinase; FH, formin homology; Lpd, lamellipodin; MEF, mouse embryonic fibroblast; Mena, mammalian Ena; MT, microtubule; Myo, myosin.

Supplemental Material can be found at:
http://www.molbiolcell.org/content/suppl/2014/06/30/mbc.E14-02-0712v1.DC1.html

filopodia formation in different cell types (Han *et al.*, 2002; Lebrand *et al.*, 2004; Mejillano *et al.*, 2004; Schirenbeck *et al.*, 2006; Applewhite *et al.*, 2007; Gates *et al.*, 2007; Homem and Peifer, 2009). They regulate actin filament architecture to favor formation of actin networks with longer, less-branched filaments by protecting filament barbed ends from capping protein (CP; Bear *et al.*, 2002; Barzik *et al.*, 2005; Pasic *et al.*, 2008). By binding processively at barbed ends, Ena/VASP proteins also promote actin monomer addition to increase the rate of actin polymerization (Breitsprecher *et al.*, 2008; Hansen and Mullins, 2010; Winkelman *et al.*, 2014). In addition, Ena/VASP may reduce Arp2/3-induced branching (Skoble *et al.*, 2001) and has been shown to induce formation of parallel actin bundles in vitro (Hüttelmaier *et al.*, 1999; Barzik *et al.*, 2005; Winkelman *et al.*, 2014). However, because filament bundling by VASP occurs only in the absence of G-actin (Hansen and Mullins, 2010), and VASP localizes to filopodia tips rather than their sides (Svitkina *et al.*, 2003; Applewhite *et al.*, 2007; Schäfer *et al.*, 2009), its side bundling activity is likely an in vitro epiphenomenon and is therefore unlikely required for filopodia formation. Because Ena/VASP proteins do not nucleate F-actin filaments under physiological conditions (Bear *et al.*, 2000; Pistor *et al.*, 2000; Barzik *et al.*, 2005), they act on filaments produced by nucleation by the Arp2/3 complex or other mechanisms (Winkelman *et al.*, 2014).

Filopodia can also be generated by members of the formin family, proteins that create unbranched filaments via de novo actin nucleation (Pruyne *et al.*, 2002). Accordingly, the Diaphanous-related formin (DRF) mDia2 nucleates linear actin filaments and opposes CP while associating processively with the growing filament barbed end and promoting rapid insertion of new actin subunits (Kovar *et al.*, 2006; Paul and Pollard, 2009). mDia2-driven filopodia formation can be activated by the small GTPases Cdc42 and Rif (Peng *et al.*, 2003; Pellegrin and Mellor, 2005). Constitutively active mDia2 induces filopodia assembly in numerous cell types (Schirenbeck *et al.*, 2005b; Wallar *et al.*, 2006; Yang *et al.*, 2007; Block *et al.*, 2008). Of note, the levels of *Drosophila* Ena and Dia affect the morphology and dynamics of actin-driven protrusions (Homem and Peifer, 2009; Bilancia *et al.*, 2014). However, it is unclear how the balance between these two actin regulators affects filopodia function. In addition, whereas the process of filopodia initiation has received considerable attention, knowledge about the physiology and regulation of mature filopodia is limited.

In this study, we used mouse embryonic fibroblasts (MEFs) that are genetically deficient for Ena/VASP and lack detectable levels of mDia2 (MV^{D7} cells) to explore the contribution of Ena/VASP and mDia2 to filopodia assembly, dynamics, and physiology in mammalian cells. Our results show that filopodia formed through pathways regulated by Ena/VASP or mDia2 have distinct properties and that both proteins have nonredundant roles in filopodia assembly and dynamics.

RESULTS

VASP and mDia2 support filopodia formation independently of one another

MV^{D7} cells were derived from mice with null alleles for endogenous Mena and VASP and selected for the absence of EVL (Bear *et al.*, 2000). MV^{D7} cells lack detectable levels of mDia1 or mDia2 but express low levels of mDia3 (Figure 1A). Thus MV^{D7} cells are a suitable model system for investigating the specific roles of Ena/VASP and mDia2 in filopodia dynamics and function.

First, we analyzed filopodia formation mediated by mDia2 in MV^{D7} cells. When expressed ectopically, green fluorescent protein (GFP)–mDia2 displayed a primarily cytoplasmic localization and did not induce filopodia formation in MV^{D7} cells (Figure 1, B, top, and C), as previously reported for other cell types (Peng *et al.*, 2003; Pellegrin and Mellor, 2005; Dent *et al.*, 2007). Given that mDia2 is regulated by an autoinhibitory mechanism (Watanabe *et al.*, 1999; Alberts, 2001; Li and Higgs, 2003, 2005), we hypothesized that MV^{D7} cells lacked the signaling pathway(s) that activate GFP-mDia2. Auto-inhibition of mDia2 is mediated by interaction between the amino (N)-terminal diaphanous inhibitory domain (DID) and the carboxy (C)-terminal diaphanous autoregulatory domain (DAD; Wallar and Alberts, 2003; Higgs, 2005; Goode and Eck, 2007; Paul and Pollard, 2009; Aspenström, 2010; Campellone and Welch, 2010; Chesarone *et al.*, 2010). We used several methods to activate ectopic mDia2 in MV^{D7} cells. Coexpression of GFP-DAD with mCherry-mDia2 in MV^{D7} cells resulted in filopodia formation, whereas GFP-DAD alone did not (Supplemental Figure S1A). Similarly, numerous filopodia were generated in MV^{D7} cells coexpressing the mDia2 activator GFP-Rif along with mCherry-mDia2 (Supplemental Figure S1B). Of note, GFP-Rif induced the formation of numerous filopodia in MV^{D7} cells by an unknown, mDia2-independent mechanism (Supplemental Figure S1B, top). Complex formation with Arp2/3 and its nucleation promoting factor (NPF) WAVE inhibits mDia2 activity, and disruption of this ternary complex induces filopodia formation (Beli *et al.*, 2008). To determine whether preventing the association of Arp2/3 with its NPFs and mDia2 would promote the formation of mDia2-dependent filopodia, we expressed the CA domain of N-WASP (Rohatgi *et al.*, 1999; Supplemental Figure S1C). The N-WASP CA region is an Arp2/3-binding sequence that is a conserved element found in all NPFs. A peptide consisting of the C-terminal CA region of N-WASP can robustly inhibit the ability of NPFs to activate Arp2/3-driven actin nucleation, presumably by blocking the interaction between Arp2/3 and its activators (Rohatgi *et al.*, 1999; Hufner *et al.*, 2001). Coexpression of GFP–N-WASP CA and mCherry-mDia2 increased filopodia formation almost threefold compared with expression of GFP–N-WASP CA or mCherry-mDia2 alone (28.1 ± 2.2 vs. 9.3 ± 0.8 and 10.0 ± 1.0 filopodia/cell, respectively; Supplemental Figure S1D). Furthermore, filopodia formed under these conditions were longer than those for cells producing GFP–N-WASP CA or mCherry-mDia2 alone (4.4 ± 0.1 vs. 2.8 ± 0.1 and 3.4 ± 0.2 µm, respectively; Supplemental Figure S1E).

Even though autoinhibited GFP-mDia2 did not increase filopodia numbers, filopodia length was subtly but significantly increased compared with control cells (Figure 1D). We conclude that although full activity of autoinhibited GFP-mDia2 required coexpression of an activator to initiate filopodia formation, it retained residual activity, resulting in slightly longer filopodia. Of importance, mDia2 activation in MV^{D7} cells does not require Ena/VASP proteins.

To simplify our analysis of mDia2-driven filopodia assembly in Ena/VASP-deficient cells, we used a previously described constitutively active mDia2 mutant, $mDia2^{M1041A}$ (referred to as $mDia2^{M/A}$ throughout this article; Wallar *et al.*, 2006). Intramolecular autoinhibition of $mDia2^{M/A}$ is neutralized by a single amino acid substitution at position 1041 in DAD (methionine to alanine). When expressed in MV^{D7} cells, GFP-$mDia2^{M/A}$ induced the formation of abundant, long filopodia and localized to the filopodia tips (Figure 1B, middle, arrowheads). In contrast, the closely related DRF paralogue mDia1, which shows 41.9% identity to mDia2, did not induce filopodia in MV^{D7} cells independently of its activation status (Supplemental Figure S2). Of note, constitutively active mDia1ΔN3 induced bleb-like structures where it colocalized with F-actin (Supplemental Figure S2, bottom). Thus only mDia2, but not mDia1, was capable of driving filopodia formation in MV^{D7} cells, and we used constitutively active $mDia2^{M/A}$ for all subsequent experiments.

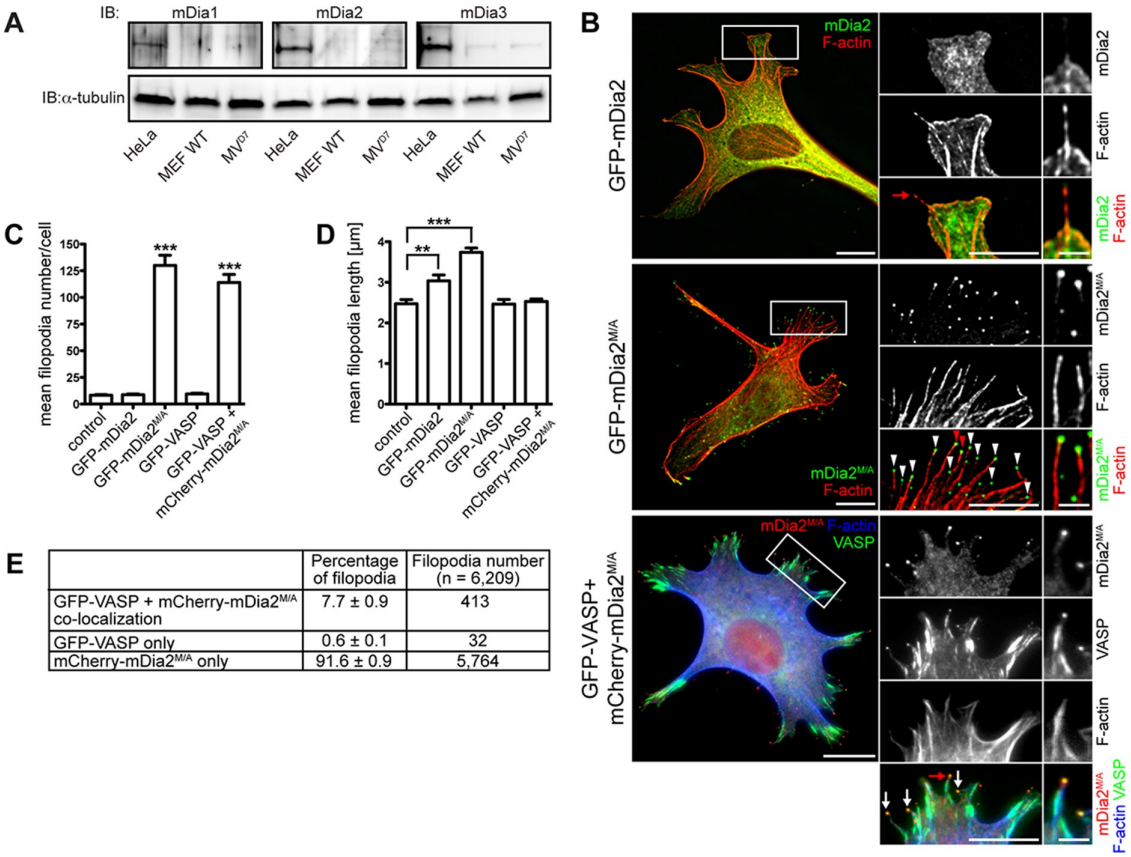

	Percentage of filopodia	Filopodia number (n = 6,209)
GFP-VASP + mCherry-mDia2$^{M/A}$ co-localization	7.7 ± 0.9	413
GFP-VASP only	0.6 ± 0.1	32
mCherry-mDia2$^{M/A}$ only	91.6 ± 0.9	5,764

FIGURE 1: Active mDia2 induces abundant long filopodia in the absence of VASP. (A) MV^{D7} cells lack endogenous mDia1 and mDia2. Cell extract from MV^{D7} cells was analyzed by SDS–PAGE and immunoblot using antibodies specific for mDia1, mDia2, or mDia3. Controls: extracts of wild-type MEFs and HeLa cells (which endogenously express mDia proteins); loading control: α-tubulin. (B) Effect of VASP and mDia2 on filopodia formation. MV^{D7} cells or MV^{D7} cells stably expressing GFP-VASP were transiently transfected with the mDia2 constructs as indicated and were chemically fixed after 24 h and probed with phalloidin to label F-actin. As expected, GFP-VASP localization to focal adhesions, lamellipodia, and filopodia tips was observed. Boxed regions represent magnified area; red arrows/arrowheads indicate filopodia magnified on the right. (C–E) Quantification of B showing mean filopodia number (C), mean length of filopodia (D), and percentage of VASP and mDia2$^{M/A}$ colocalization at filopodia tips in cells coexpressing GFP-VASP and mCherry-mDia2$^{M/A}$ (E). Data in C–E represent at least two repetitions. ***$p \leq 0.001$, **$p \leq 0.01$; $n = 33$–59 cells. Scale bars, 15 µm; magnified regions, 5 µm; single filopodia, 1 µm.

GFP-mDia2$^{M/A}$ expression increased filopodia numbers >13-fold compared with nontransfected cells or to those expressing GFP-VASP or autoinhibited GFP-mDia2 (Figure 1C), and the filopodia were significantly longer (Figure 1D). Similar to GFP-mDia2$^{M/A}$ expression, coexpression of mCherry-mDia2$^{M/A}$ with GFP-VASP in MV^{D7} cells induced large numbers of filopodia that were primarily labeled by mCherry-mDia2$^{M/A}$ at the tip (91.6 ± 0.9%; Figure 1E). Filopodia numbers in cells coexpressing both proteins were not further increased compared with expression of GFP-mDia2$^{M/A}$ alone, arguing against additive effects of VASP and mDia2$^{M/A}$ on actin filament assembly during filopodium formation. In 7.7 ± 0.9% of filopodia (Figure 1E), VASP and mDia2$^{M/A}$ colocalized to filopodium tips (Figure 1B, bottom, arrows), consistent with their ability to bind actin filament barbed ends (Bear *et al.*, 2002; Zigmond *et al.*, 2003; Kovar and Pollard, 2004; Moseley *et al.*, 2004; Pasic *et al.*, 2008; Hansen and Mullins, 2010). Of note, filopodia containing both GFP-VASP and mCherry-mDia2$^{M/A}$ assembled in cells coexpressing both proteins were significantly shorter and comparable in length to filopodia formed in control cells or cells expressing GFP-VASP (Figure 1D). Thus VASP expression may restrain the length of filopodia formed by mDia2$^{M/A}$.

We next investigated the molecular composition of filopodia formed in mDia2$^{M/A}$- or VASP-expressing cells. Filopodia in MV^{D7} cells expressing either GFP-VASP or GFP-mDia2$^{M/A}$ contained actin filaments (Figure 1B, middle) cross-linked by the actin bundler fascin, a canonical marker of the filopodium/microspike shaft (Kureishy *et al.*, 2002; Svitkina *et al.*, 2003; Figure 2A). Similarly, lamellipodin (Lpd), a marker that localizes to the tips of lamellipodia and filopodia (Krause *et al.*, 2004; Figure 2B), and the filopodia tip markers myosin X (MyoX) (Bohil *et al.*, 2006) and phosphotyrosine (pTyr; Wu and Goldberg, 1993) were detectable in all filopodia (Supplemental Figure S3, A and B). Thus, although GFP-mDia2$^{M/A}$–assembled filopodia are longer and more numerous than those formed in GFP-VASP–expressing cells, their molecular composition was similar. Of interest, Lpd labeling revealed that GFP-mDia2$^{M/A}$ expression reduced the percentage of the cell perimeter composed of lamellipodium-like structures by ~50% (Lpd-labeled cell edge [%]: GFP-mDia2$^{M/A}$-expressing cells, 13.2 ± 2.4 vs. control cells, 26.0 ± 2.8, or GFP-VASP-expressing cells, 25.1 ± 1.2; Figure 2, B and C). Staining for a second lamellipodial marker, cortactin, yielded similar results (Supplemental Figure S3C). Thus, in the absence of Ena/VASP proteins, mDia2$^{M/A}$

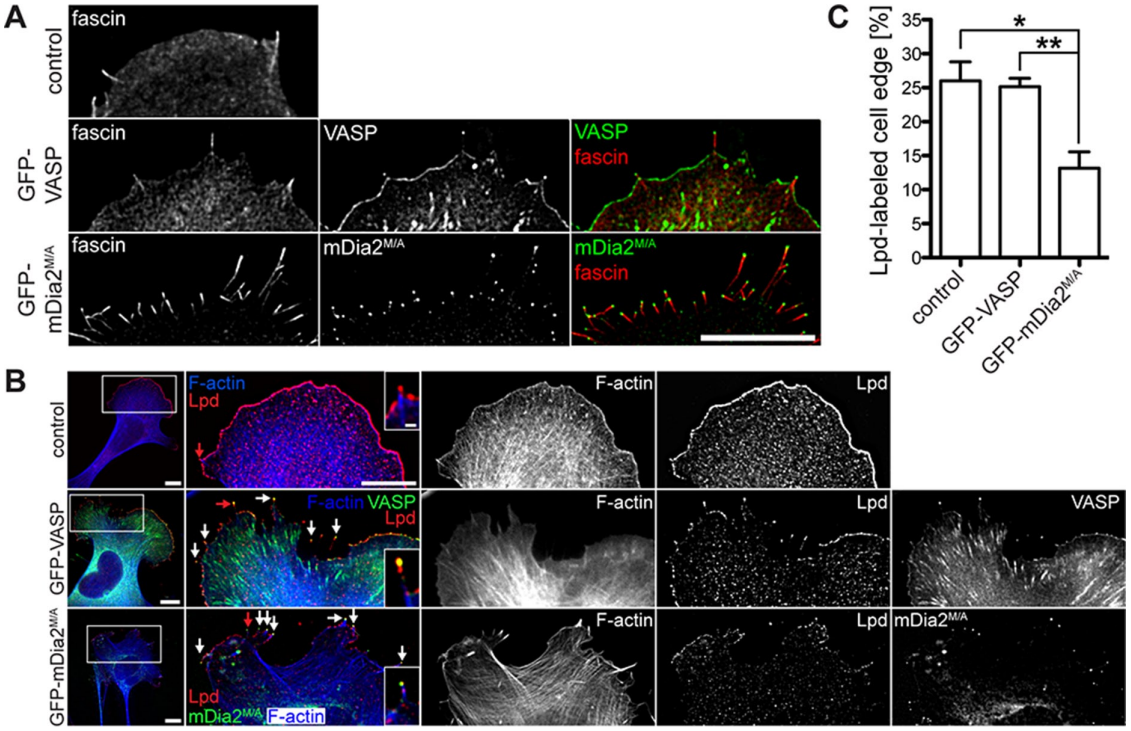

FIGURE 2: MV^{D7} cells expressing mDia2$^{M/A}$ have smaller lamellipodia. (A) MV^{D7} cells expressing mDia2$^{M/A}$ contain the normal filopodia inventory. MV^{D7} cells producing the indicated proteins were chemically fixed and stained for the actin cross-linking protein fascin. (B) Lpd antibody labels filopodia tips (arrows) and the actively protruding leading edge of lamellipodia. Right, magnification of boxed regions. Red arrows indicate filopodia magnified in insets. (C) Quantification of Lpd-labeled cell edge from experiments shown in B. Cells were transiently transfected, fixed, and stained with Lpd antibody. Data in C represent at least two repetitions. *$p \leq 0.05$, **$p \leq 0.01$; $n = 10$–13 cells. Scale bars, 15 μm; magnified images, 5 μm; single-filopodium insets, 1 μm.

appears to promote extensive filopodia assembly at the expense of lamellipodium formation.

Ena/VASP and mDia2 interact directly through Ena/VASP homology 1–formin homology 2 interactions

Given that 1) mDia2$^{M/A}$ and VASP colocalize to filopodium tips (Figure 1B), 2) the Dictyostelium VASP and Dia2 orthologues interact directly in vitro (Schirenbeck *et al.*, 2006), and 3) the *Drosophila* orthologues interact in fly embryos (Homem and Peifer, 2009), we tested whether Ena/VASP forms a complex with mDia2 in mammalian cells. The N-terminal Ena/VASP homology (EVH) 1 domain recognizes four FPPPP (FP4) motifs from *Listeria monocytogenes* ActA (Niebuhr *et al.*, 1997), and transiently expressed mitochondrial-targeted FP4 motifs (FP4-mito) can relocalize Ena/VASP to the mitochondrial surface (Bear *et al.*, 2000). As expected, FP4-mito sequestered endogenous Ena/VASP proteins to mitochondrial membranes in NIH3T3 cells (Figure 3A). Without FP4-mito expression, Mena and GFP-mDia2 localized normally (Figure 3A, top). In cells producing FP4-mito, Mena and constitutively active GFP-mDia2$^{M/A}$ (Figure 3A, bottom), but not autoinhibited GFP-mDia2, were recruited to mitochondria (Figure 3A, middle). Quantification of the colocalization between Mena and GFP-mDia2 by Pearson's *r* confirmed a significant ($p < 0.01$) decrease of Mena's colocalization with autoinhibited GFP-mDia2, as Mena was sequestered to mitochondria by FP4-mito, whereas GFP-mDia2 remained in the cytoplasm. Such a decrease was not seen in cells expressing GFP-mDia2$^{M/A}$, as both proteins were corecruited to mitochondria (Figure 3B). Together these data indicate that Ena/VASP exists in a complex with active but not autoinhibited mDia2 in living cells.

Because ectopic expression of wild-type mDia2 drives filopodia formation in Ena/VASP-deficient neurons (Dent *et al.*, 2007), we hypothesized that neurons contain all signaling components to activate mDia2. Indeed, expression of FP4-mito in wild-type cortical neurons efficiently recruited both autoinhibited GFP-mDia2 and activated GFP-mDia2$^{M/A}$ to mitochondria, and this sequestration most likely occurred through endogenous Ena/VASP proteins (Supplemental Figure S4). Thus certain specialized cells such as neurons may facilitate association of mDia2 with Ena/VASP by enabling mDia2 activation. However, in fibroblasts (such as NIH3T3 and MV^{D7} cells), the interaction between Ena/VASP and mDia2 is tightly regulated by mDia2's activation status and is precluded when mDia2 is autoinhibited.

Next we explored whether Ena/VASP binds directly to mDia2$^{M/A}$. Using purified recombinant proteins, we found that the immobilized glutathione-*S*-transferase (GST) formin homology (FH) 2 domain of mDia2 retained purified hexahistidine (His_6)-VASP on glutathione Sepharose (GS) beads (Figure 3C), whereas immobilized GST did not. Because binding to the N-terminal EVH1 domain in Ena/VASP typically occurs through a proline-rich consensus motif FPPPP (Niebuhr *et al.*, 1997; Carl *et al.*, 1999; Ball *et al.*, 2000), we tested whether a similar FPPP motif in the FH2 domain of mDia2 (amino acids 918–921) was required for interaction with the VASP EVH1 domain. Deletion of the VASP EVH1 domain (Figure 3D) or substitution of a single side chain within the canonical EVH1-binding motif in mDia2 FH2 (F918D; Figure 3E) abrogated interactions between Ena/VASP and mDia2$^{M/A}$. Together our data strongly suggest that the mDia2 FH2 domain binds directly to the EVH1 domain of Ena/VASP proteins through the FPPP motif.

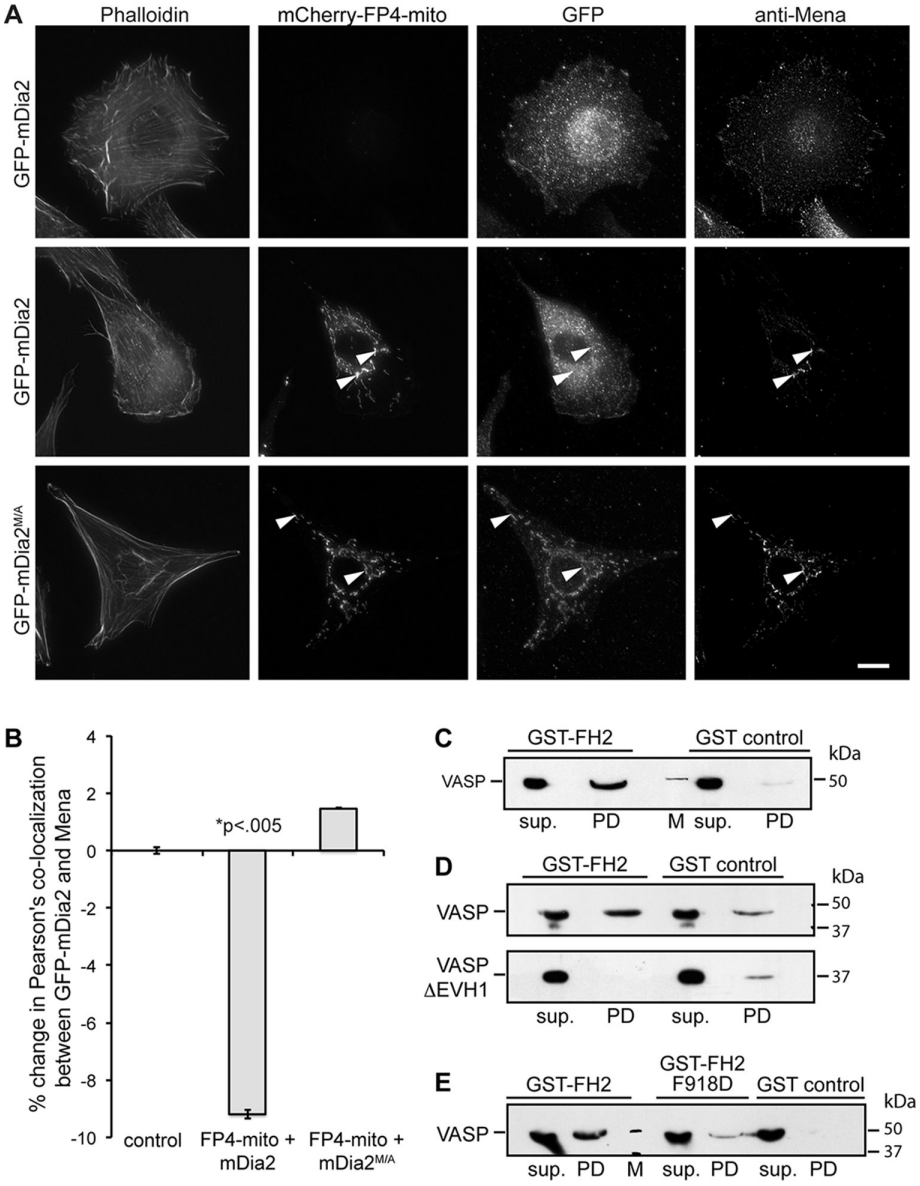

FIGURE 3: VASP directly interacts with mDia2. (A) Mitochondria-targeting assay. Transiently transfected NIH3T3 cells producing the indicated GFP- or mCherry-tagged proteins were chemically fixed and probed with a marker for F-actin (phalloidin) or antibody directed against Mena. Arrowheads indicate mitochondria labeled with mCherry-FP4-mito. Scale bar, 15 μm. (B) Quantification of A showing percentage change in Pearson's colocalization coefficient between Mena and GFP-mDia2. (C–E) Pull-down studies analyzing complex formation between mDia2 and VASP. Bead-immobilized GST-FH2 domain was incubated with purified VASP or VASPΔEVH1, and protein retained on beads was detected by SDS–PAGE and immunoblot. sup., supernatant; PD, pull down; M, molecular weight marker. (C) VASP interacts with the mDia2 FH2 domain. (D) VASP binds mDia2 through its EVH1 domain. (E) The FPPP motif in mDia2 FH2 mediates interaction with VASP. All data are from at least three independent experiments.

Filopodia formed in MV^{D7} cells expressing VASP and mDia2 display distinct dynamics

Given the dynamic nature of actin-based protrusions, we performed live-cell time-lapse microscopy of VASP- or mDia2$^{M/A}$-containing filopodia. GFP-VASP and GFP-mDia2$^{M/A}$ localized to protruding tips of filopodia (Figure 4A and Supplemental Movies S1 and S2), consistent with their continuous association with elongating filament barbed ends (Svitkina *et al.*, 2003; Yang *et al.*, 2007). Nascent filopodia in GFP-VASP–expressing cells protruded unidirectionally from the extending lamellipodium edge (Figure 4A, top, and Supplemental Movie S1). In contrast, filopodium dynamics in GFP-mDia2$^{M/A}$–expressing cells was highly irregular: these filopodia frequently collapsed backward onto the cell and repeatedly changed directions (Figure 4A, middle, and Supplemental Movie S2). Consequently the lifetime of filopodia assembled by GFP-mDia2$^{M/A}$ was almost 1.5-fold shorter than with VASP-containing filopodia (Figure 4B). We next investigated whether the inconsistent directionality of mDia2$^{M/A}$-assembled filopodia affected their protrusive persistence (continual directional movement over time; see *Materials and Methods*; Figure 4D). Protrusive persistence of GFP-VASP–labeled filopodia was high, whereas that of GFP-mDia2$^{M/A}$–induced filopodia was nearly threefold lower (Figure 4C), suggesting that inconsistent directionality of mDia2$^{M/A}$-assembled filopodia reduces effective filopodium protrusion.

Because VASP reduced filopodium length in mDia2$^{M/A}$-expressing cells (Figure 1D), we tested whether VASP coexpression rescued the aberrant dynamics of mDia2$^{M/A}$-induced filopodia. In cells expressing both proteins, two filopodia types were observed (Figure 1A and Supplemental Movie S3): 1) long, mCherry-mDia2$^{M/A}$–labeled filopodia, which switched directions frequently and displayed almost 2-fold-reduced protrusive persistence and 1.6-fold-reduced lifetime, and 2) filopodia containing both GFP-VASP and mCherry-mDia2$^{M/A}$, which extended steadily in a consistent direction, with protrusive persistence and lifetime comparable to filopodia containing VASP alone (Figure 4, A, arrowheads, B, and C). Thus directionality of filopodial tip movement, required for stable protrusion of filopodia, as well as filopodia lifetime, is conferred by VASP but not by mDia2$^{M/A}$.

Cytoskeletal reorganization has to be coupled to cell–matrix adhesions to generate the traction forces that promote protrusion and cell motility (Schiller and Fässler, 2013). Nascent focal complexes have been observed to assemble at both the tip (Schäfer *et al.*, 2009) and base of emerging filopodia (Steketee *et al.*, 2001), whereas filopodia lacking proper adhesion tend to retract (Mallavarapu and Mitchison, 1999). We used the focal adhesion core protein GFP-zyxin to test whether cells coexpressing mCherry-mDia2$^{M/A}$ or mCherry-VASP formed stable cell–matrix contacts during filopodia extension (Figure 4E and Supplemental Movies S4 and S5). Coexpression of GFP-zyxin did not alter protrusive persistence, confirming that the construct had no effect on filopodia dynamics (Figure 4F). In the presence of mCherry-VASP, filopodia appeared to mark sites of nascent focal contact formation (Figure 4E, top, arrows, Supplemental Figure S5, and Supplemental Movie S6) with an average of 1.2 ± 0.1 de novo focal adhesions/filopodium being formed (Figure 4G). In cells coexpressing mCherry-mDia2$^{M/A}$, GFP-zyxin–labeled

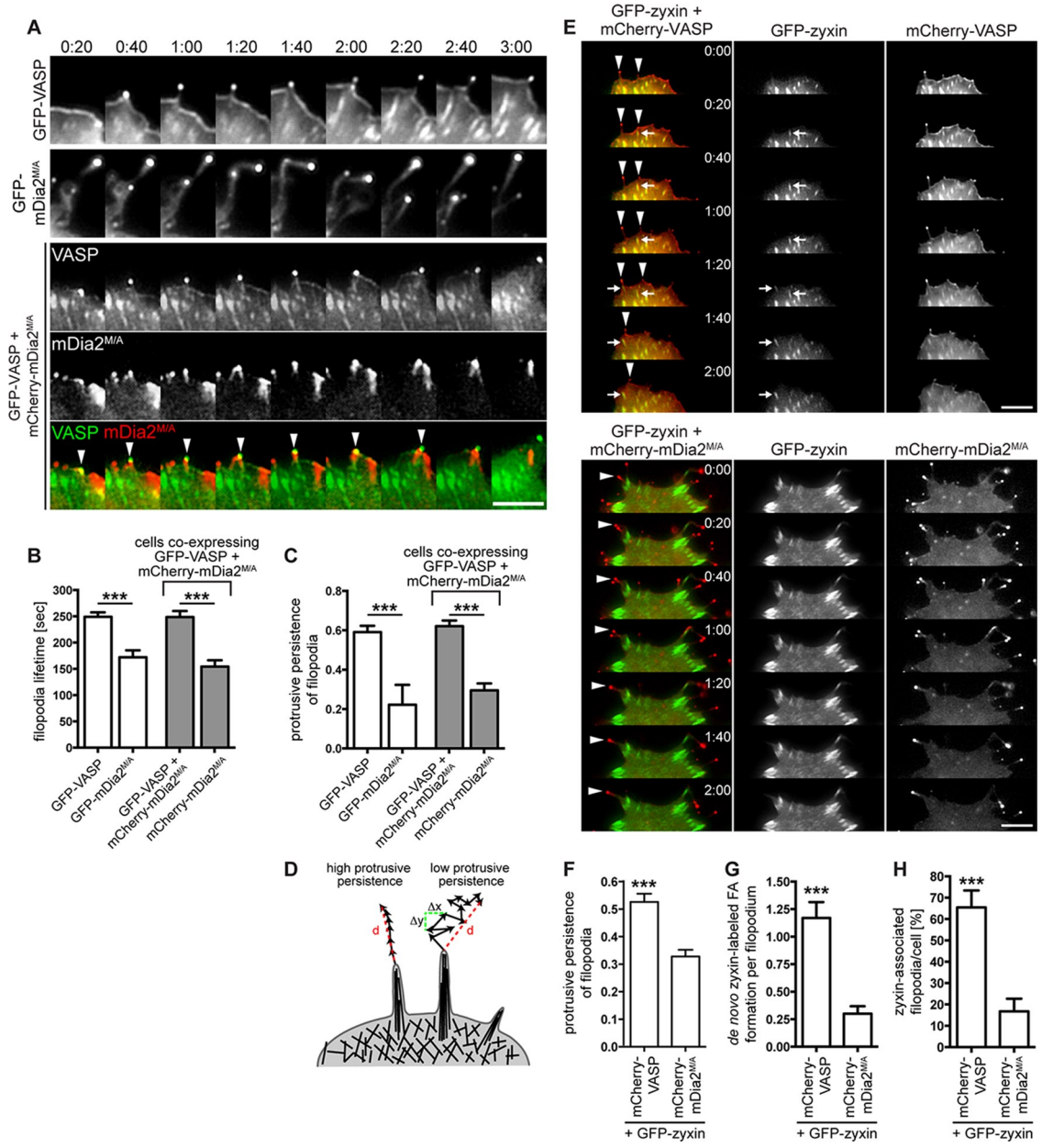

FIGURE 4: VASP is essential for persistent protrusion of mDia2-generated filopodia. (A) VASP restores protrusive behavior of mDia2$^{M/A}$-induced filopodia. MV^{D7} cells were transfected as indicated and plated on fibronectin-coated glass bottom dishes for 24 h before live-cell imaging. Montages of single frames from 3:00 min of live-cell microscopy time series. (B, C) Quantification of protrusive persistence (B) and lifetime (C) of filopodia from experiments shown in A. Filopodia tips in cells expressing GFP-VASP, GFP-mDia2$^{M/A}$, or GFP-VASP plus mCherry-mDia2$^{M/A}$ were tracked in individual frames of 5-min movies, and so were filopodia that were in the same coexpressing cells but that contained only mCherry-mDia2$^{M/A}$. Data represent at least two repetitions. n = 7–16 cells. (D) Distinct filopodia dynamics results in variable protrusive persistence. Protrusive persistence of filopodia was calculated by measuring the total distance (d) traveled by the filopodium tip divided by the sum of the change in directionality (Δx, Δy) of the filopodium tip between individual frames (see *Materials and Methods*). (E–H) VASP- but not mDia2$^{M/A}$-containing filopodia (arrowheads) induce de novo assembly of GFP-zyxin–labeled focal adhesions at their base or in the shaft while actively protruding (arrows). MV^{D7} cells were transfected as indicated and plated on fibronectin-coated glass-bottom dishes for 24 h before live-cell imaging. (E) Montages of single frames from 2 min of live-cell microscopy time series. (F) GFP-zyxin expression does not change filopodia dynamics. (G) Quantification of de novo focal adhesion formation in protruding filopodia from experiments shown in E. (H) Percentage of zyxin-associated filopodia/cell. Data in F–H represent at least two repetitions. N = 8–11 cells, n = 41–60 filopodia in F and G; n = 58 (VASP) and 1426 (mDia2$^{M/A}$) filopodia in H. ***$p < 0.001$. Scale bars, 5 μm.

focal adhesions often localized immediately behind the cell periphery and appeared to coincide with the base of filopodia (Figure 4E, bottom). This arrangement was most likely caused by the reduction of the lamellipodium (Figure 2C), where matrix adhesions usually assemble and mature (Zaidel-Bar *et al.*, 2003; Alexandrova *et al.*, 2008). However, de novo assembly of GFP-zyxin–labeled focal adhesions

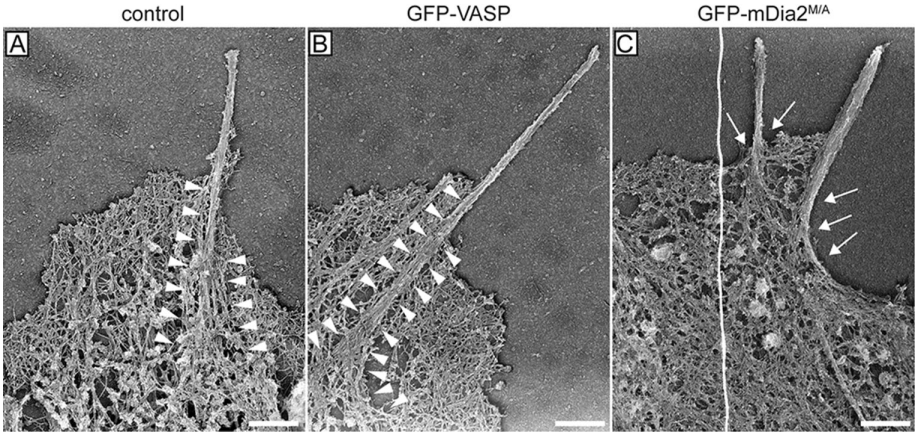

FIGURE 5: Actin bundles in filopodia initiated by mDia2$^{M/A}$ are not anchored in the lamellipodium actin network. Representative platinum-replica electron micrographs of actin cytoskeletons from MV^{D7} cells. Filopodium F-actin bundles from control cells (A) and cells complemented with GFP-VASP (B) are deeply embedded in the actin network of the lamellipodium (arrowheads) and splay apart at the filopodium root. In contrast, filopodia actin bundles of cells producing GFP-mDia2$^{M/A}$ (C) display poor connection to the underlying cortical cytoskeleton and do not have splayed roots (arrows), indicating that they may have formed via a different mechanism. Electron micrographs are representative images from at least three independent experiments. Scale bars, 0.5 μm.

at the base or along the shaft of actively elongating filopodia was significantly reduced in mCherry-mDia2$^{M/A}$–expressing cells (0.3 ± 0.1 focal adhesions/filopodium; Figure 4G). Consequently the percentage of GFP-zyxin–labeled puncta associated with filopodia was almost fourfold reduced in MV^{D7} cells expressing mCherry-mDia2$^{M/A}$ (16.8 ± 1.8%) compared with mCherry-VASP–expressing cells (65.5 ± 7.9%; Figure 4H). Thus assembly of nascent adhesion sites in mDia2$^{M/A}$-generated filopodia may be impaired, which could also result in reduced extensions of cell protrusions.

Accordingly, MV^{D7} cells expressing GFP-mDia2$^{M/A}$ exhibited a substantial reduction of lamellipodial area (Figure 2, B and C), a phenotype that could arise from adhesion defects, aberrant actin polymerization, or both. Analysis of the F-actin architecture of filopodia by platinum-replica electron microscopy showed that filopodia of control MV^{D7} cells, or cells expressing GFP-VASP, contained thick bundles of long, parallel F-actin filaments embedded deeply within the lamellipodial network (arrowheads in Figure 5, A and B). In contrast, actin bundles in GFP-mDia2$^{M/A}$–expressing cells arose directly from the cortical cytoskeleton (arrows in Figure 5C) and did not appear to be connected to the underlying actin networks.

Taken together, our data suggest that actin filaments in GFP-mDia2$^{M/A}$–assembled filopodia are insufficiently anchored within the underlying cytoskeleton. This lack of structural support in combination with increased filament length most likely resulted in diminished filopodial stability. This hypothesis is supported by our observations of irregular dynamics, reduced lifetime, and diminished protrusive persistence of mDia2$^{M/A}$-initiated filopodia. We further hypothesize that the structural instability and resulting irregular dynamics of mDia2$^{M/A}$-induced filopodia also caused a reduction of filopodia-initiated substrate adhesion sites, which itself resulted in a reduction of lamellipodium area and overall protrusion.

Microtubules exploring mDia2$^{M/A}$-induced filopodia increase filopodium length but are not required for filopodium assembly

Constitutively active deletion mutants of mDia2 stabilize microtubules in cultured cells and bind directly to microtubules in vitro (Palazzo *et al.*, 2001; Wen *et al.*, 2004; Bartolini *et al.*, 2008). We thus explored whether association with microtubules contributed to the dynamic properties of mDia2$^{M/A}$-assembled filopodia in MV^{D7} cells. Indeed, 57.0 ± 2.8% of GFP-mDia2$^{M/A}$–labeled filopodia contained microtubules (Figure 6, A, arrows, and D). Of note, these microtubules (MTs) were dynamic, tyrosinated (Tyr-MTs) but not stabilized, detyrosinated microtubules (Glu-MTs; Supplemental Figure S6A). Furthermore, colocalization of dynamic microtubules with F-actin bundles suggested an engagement of the actomyosin cytoskeleton in these GFP-mDia2$^{M/A}$–induced filopodia (Supplemental Figure S6B). Microtubules were rarely present in filopodia of MV^{D7} control or GFP-VASP cells (<4%) (Figure 6, A, arrowheads, and D). Coexpression of fluorescent microtubule plus end–binding protein (+TIP) EB1 to mark actively growing microtubule tips, followed by time-lapse imaging, confirmed that dynamic microtubules enter and then persist within GFP-mDia2$^{M/A}$–assembled filopodia (Figure 6B, bottom, arrowheads, and Supplemental Movie S7), indicating that microtubules actively polymerize while protruding into filopodia of mDia2$^{M/A}$-expressing cells. EB1 did not enter VASP-containing filopodia, demonstrating that growing microtubules are not associated with the formation or elongation of VASP-labeled filopodia in fibroblasts (Figure 6B, top, and Supplemental Movie S8).

To assess whether mDia2$^{M/A}$-driven filopodia assembly is dependent on microtubule dynamics, we incubated MV^{D7} cells with nocodazole, which caused robust microtubule depolymerization (Figure 6C, bottom, and D; <1% microtubule-containing filopodia). Filopodia assembly was not inhibited by microtubule depolymerization in cells expressing GFP-VASP (number of filopodia/cell: nocodazole, 14.7 ± 1.1 vs. DMSO control, 11.6 ± 0.9; Figure 6E). Although nocodazole treatment resulted in robust microtubule depolymerization in cells expressing GFP-mDia2$^{M/A}$, these cells continued to form abundant filopodia (nocodazole, 143.8 ± 11.5 vs. DMSO control, 120.2 ± 7.6; Figure 6, C–E). Thus microtubules are not required for assembly or maintenance of GFP-mDia2$^{M/A}$–initiated filopodia. Of note, GFP-mDia2$^{M/A}$ was still localized to filopodium tips in nocadazole-treated cells, demonstrating that microtubules are also not required to target GFP-mDia2$^{M/A}$ to filopodia tips (Figure 6C). Of interest, in the absence of microtubules, GFP-mDia2$^{M/A}$–initiated filopodia were almost twofold shorter (nocodazole, 2.5 ± 0.1 μm vs. DMSO control, 4.7 ± 0.1 μm), whereas GFP-VASP–initiated filopodia were slightly longer compared with control cells (nocodazole, 2.7 ± 0.1 μm vs. DMSO control, 2.2 ± 0.1 μm; Figure 6F). Thus, whereas microtubules affect elongation of GFP-mDia2$^{M/A}$–initiated filopodia, they are required for neither mDia2$^{M/A}$-driven filopodia formation nor localization of GFP-mDia2$^{M/A}$ to filopodial tips.

mDia2-assembled filopodia do not support early cell spreading

Given that cell spreading occurs by assembly of initial focal contacts between filopodia and the substrate (Partridge and Marcantonio, 2006) and that de novo formation of focal adhesions in filopodia of

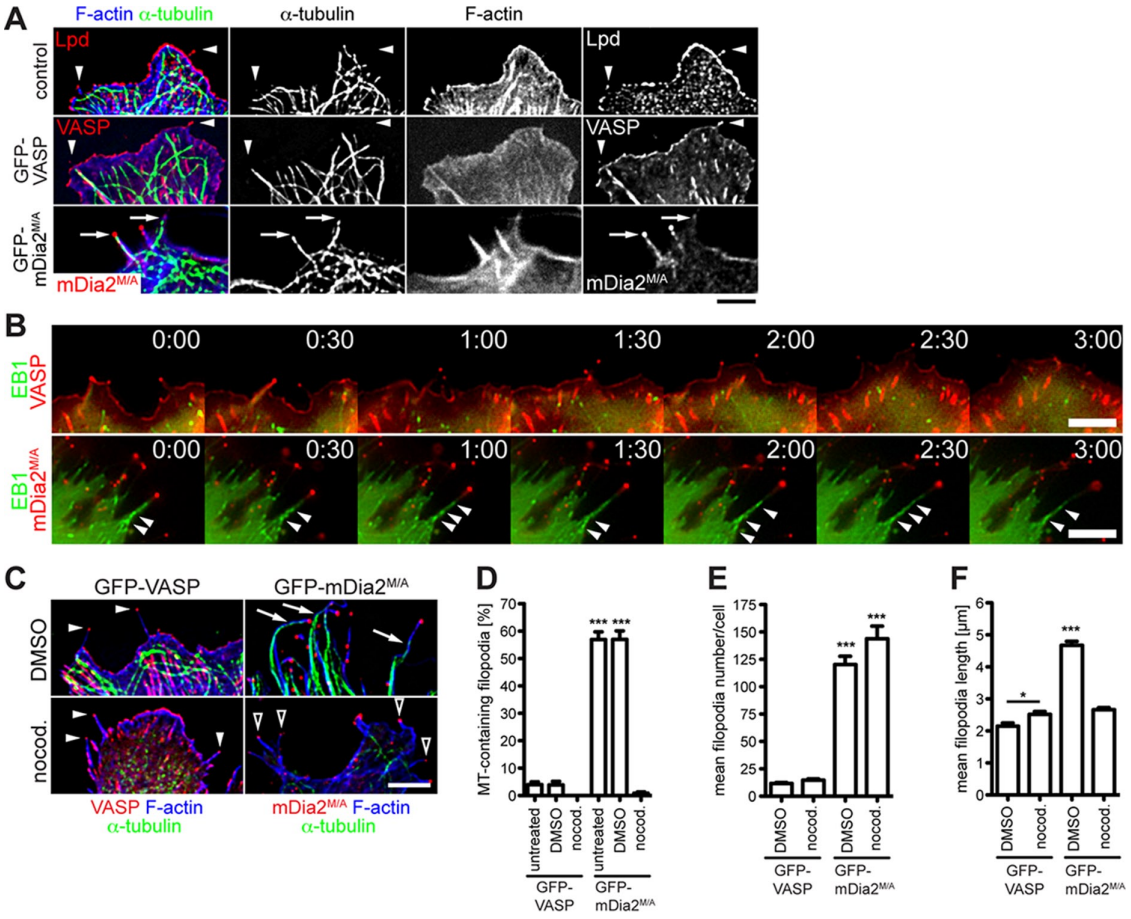

FIGURE 6: Microtubule targeting of mDia2$^{M/A}$-initiated filopodia. (A) mDia2$^{M/A}$-assembled filopodia contain microtubules. MV^{D7} cells were transiently transfected, chemically fixed, and probed for microtubules (α-tubulin), filopodia (Lpd), and F-actin (phalloidin). Arrows indicate microtubules extending into tips of mDia2$^{M/A}$-assembled filopodia. Arrowheads show that microtubules do not extend into filopodia of control or GFP-VASP–expressing cells. (B) Actively polymerizing microtubules perpetually protrude into mDia2$^{M/A}$-induced filopodia. Montages of single frames from 3-min time series of cells coexpressing mCherry-EB1 and either GFP-VASP (top) or GFP-mDia2$^{M/A}$ (bottom). Arrowheads indicate EB1-labeled microtubules actively entering mDia2$^{M/A}$-labeled filopodia. (C) Filopodia in GFP-VASP–expressing (left) or GFP-mDia2$^{M/A}$–expressing (right) cells are unaffected by microtubule depolymerization. Transfected cells were exposed to 100 ng/ml nocodazole for 15 h (DMSO control, top; nocodazole, bottom) and probed for α-tubulin and F-actin (phalloidin). Nocodazole does not affect filopodia formation in GFP-VASP–expressing cells (filled arrowheads). DMSO treatment does not prevent microtubules from entering GFP-mDia2$^{M/A}$–labeled filopodia (arrows). Depolymerization of microtubules does not inhibit filopodia formation in cells expressing GFP-mDia2$^{M/A}$ but reduces filopodial length (open arrowheads). (D–F) Quantification of the experiments shown in A and C. (D) mDia2$^{M/A}$-labeled filopodia do not contain microtubules in nocodazole-treated cells. (E) Microtubules are not required for GFP-mDia2$^{M/A}$–driven filopodia formation. (F) Microtubule depolymerization dramatically reduces filopodia length in cells expressing GFP-mDia2$^{M/A}$, whereas filopodial length in GFP-VASP–expressing cells is slightly increased. Data in D–F represent at least two repetitions. *$p < 0.05$; ***$p < 0.001$. DMSO, vehicle control; nocod., nocodazole. $n = 39$–55 cells. Scale bars, 5 μm.

GFP-mDia2$^{M/A}$–expressing cells was impaired (Figure 4G), we asked whether mDia2$^{M/A}$ affects cell spreading, using a previously established assay for cell spreading and filopodia formation in MV^{D7} cells plated on laminin (Applewhite *et al.*, 2007). Spreading MV^{D7} control cells and those expressing GFP-VASP displayed isotropic extension of a mostly smooth, circular lamellipodium with embedded short filopodia and microspikes (Figure 7, A and B) and comparable spreading efficiency after 30 min (cell area: control, 1297 ± 60 μm^2 vs. GFP-VASP, 1082 ± 42 μm^2; Figure 7F). In contrast, GFP-mDia2$^{M/A}$ expression severely impaired spreading efficiency, with a cell area reduction by >50% (488 ± 37 μm^2; Figure 7, C and F). We hypothesized that either high numbers of filopodia interfered with cell spreading or properties of GFP-mDia2$^{M/A}$–assembled filopodia impeded cell spreading. To differentiate between these possibilities, we analyzed spreading of MV^{D7} cells expressing GFP-MyoX. Similar to GFP-mDia2$^{M/A}$, GFP-MyoX induced increased numbers of long filopodia and localizes to their tips (Supplemental Figure S7). However, abundant filopodia did not compromise spreading of cells expressing GFP-MyoX (1246 ± 118 μm^2; Figure 7, E and F), indicating that inherent properties of GFP-mDia2$^{M/A}$–initiated filopodia impaired cell spreading. Consistent with this, coexpression of VASP partially rescued the spreading defect of mDia2$^{M/A}$-expressing cells (811 ± 62 μm^2), despite the presence of numerous long mDia2$^{M/A}$-containing (and GFP-VASP deficient) filopodia along with the shorter, persistent filopodia containing both mDia2$^{M/A}$ and VASP (Figure 7, D and F). Comparable to our observations on steady-state

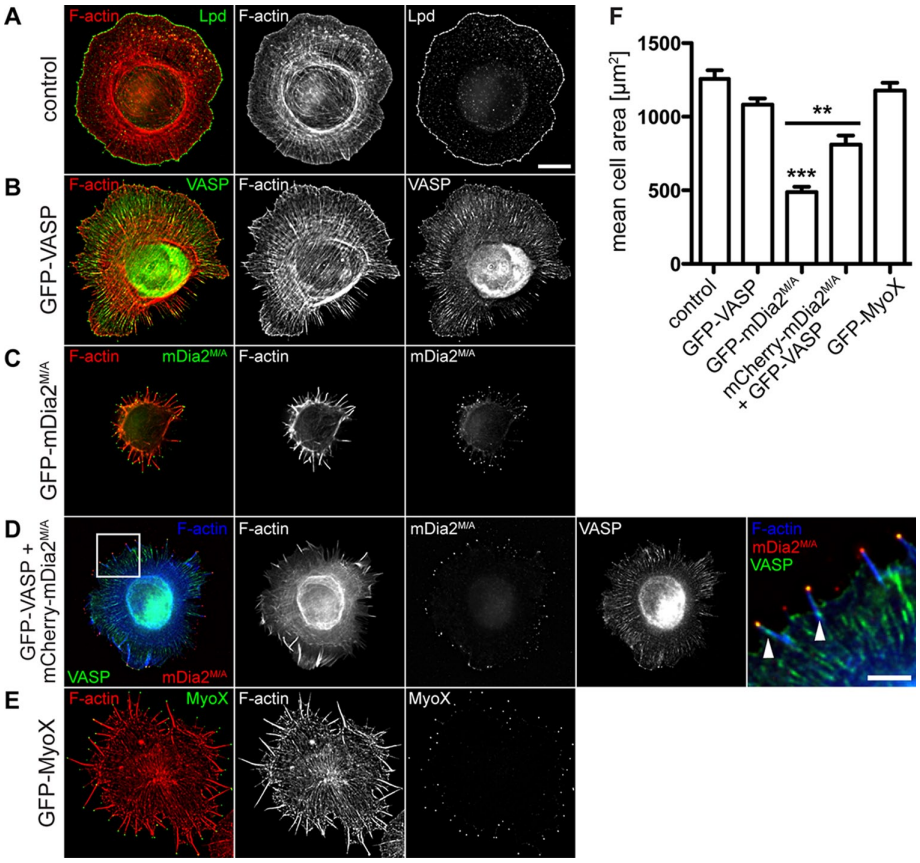

FIGURE 7: Filopodia initiated by mDia2$^{M/A}$ do not support early cell spreading. (A–E) Cell spreading assay. At 24 h after transfection, MV^{D7} control cells (A) or MV^{D7} cells producing (B) GFP-VASP, (C) GFP-mDia2$^{M/A}$, (D) GFP-VASP + mCherry-mDia2$^{M/A}$, or (E) GFP-MyoX were allowed to spread on laminin-coated coverslips for 30 min and fixed, and F-actin was labeled with phalloidin. Control cells were also probed with antibody directed against Lpd. Box in D shows localization of magnified region on the right, where small focal adhesions labeled by GFP-VASP at the base of filopodia are indicated by arrowheads. (F) Quantification of cell area from cell spreading assays as depicted in A–E. Data represent at least two independent experiments. ***$p < 0.001$; **$p < 0.01$. $n = 43$-45 cells. Scale bar, 15 µm; magnified image, 5 µm.

cells, platinum-replica electron microscopy of actin cytoskeletons from spreading cells showed that GFP-mDia2$^{M/A}$–assembled filopodia arose directly from the cortical actin network and were often bent (Supplemental Figure S8, E–G). In addition, these filopodia were rarely connected to small lamellipodium-like protrusions, whereas in control and GFP-VASP–expressing cells, filopodia originated deep within lamellipodia and extended straight from the leading edge (Supplemental Figure S8, A–D).

Because filopodia can also serve as precursors for lamellipodium formation during cell spreading (Guillou *et al.*, 2008), and lamellipodia formation in GFP-mDia2$^{M/A}$–expressing MV^{D7} cells is significantly diminished under steady-state conditions (Figure 2, B and C), we assessed whether lamellipodium formation was similarly affected in spreading cells. Staining for Lpd showed a reduction of the lamellipodium area in spreading GFP-mDia2$^{M/A}$ cells; however, in spreading control and GFP-VASP cells, a ring-like Lpd localization at the leading edge revealed a protrusive lamellipodium spanning the entire circumference (Figure 8A). Thus abundant GFP-mDia2$^{M/A}$–assembled filopodia appear to interfere with lamellipodium formation and protrusion during spreading, further indicating that they are functionally distinct from VASP-containing filopodia.

Consistent with a spreading defect, phalloidin labeling of the actin cytoskeleton revealed that MV^{D7} cells expressing GFP-mDia2$^{M/A}$ were almost completely devoid of both contractile actin stress fibers and the actin bundles parallel to the cell edge typically generated by myosin II activity, known as actin arcs (Burnette *et al.*, 2011; Figure 7C). However, contractile F-actin structures were observed in control and GFP-VASP cells (Figure 7, A and B). Of importance, coexpression of VASP rescued formation of contractile F-actin structures in mDia2$^{M/A}$-expressing cells (Figure 7D). Thus our data suggest that GFP-mDia2$^{M/A}$–expressing MV^{D7} cells fail to assemble contractile F-actin networks during the early spreading phase. This cytoskeletal contractility defect likely contributed to the decreased formation of protrusive lamellipodia and compromised spreading of cells lacking VASP.

GFP-mDia2$^{M/A}$–assembled filopodia do not support formation of initial focal contacts

Contractile forces must link to adhesion sites for efficient membrane protrusion and cell migration during spreading. Early in adhesion, activation of integrin receptors establishes a physical link between the extracellular matrix (ECM) and the actin cytoskeleton (Tamkun *et al.*, 1986; Huttenlocher *et al.*, 1996). During cell spreading, initial integrin-containing adhesion sites are assembled in filopodia (Partridge and Marcantonio, 2006). The defect in formation of zyxin-labeled focal adhesions (Figure 4G) and reduction of contractile actin stress fibers and myosin II–generated actin arcs in GFP-mDia2$^{M/A}$ cells (Figure 7C) led us to examine whether mDia2$^{M/A}$-assembled filopodia can initiate integrin-dependent cell-matrix contacts during early spreading. Because most laminin-binding integrins contain β1 subunits (Hynes, 2002), we examined spreading cells by immunofluorescence staining with conformation-state-sensitive anti–β1-antibodies. Activated β1 integrin localized in a dot-like pattern in the cell body but not to filopodia shafts or tips in GFP-mDia2$^{M/A}$ cells (Figure 8B, bottom). In contrast, GFP-VASP and activated β1 integrin were frequently colocalized at elongated focal adhesions and at filopodia tips (Figure 8B, middle, arrows). Thus ECM engagement leads to β1 integrin activation only at tips of GFP-VASP–assembled filopodia but not at tips of GFP-mDia2$^{M/A}$–initiated filopodia.

To assess whether integrin-dependent signaling pathways required for formation of focal contacts and adhesions are activated during cell spreading, we tested for integrin-induced autophosphorylation on Tyr-397 of focal adhesion kinase (FAK), an initial step in FAK activation (Katz *et al.*, 2002; Parsons, 2003; Shi and Boettiger, 2003). Consistent with deficient integrin activation, pFAK^{397} localized diffusely to the cytoplasm of GFP-mDia2$^{M/A}$–expressing cells, whereas it labeled focal contacts and focal adhesions in lamellipodia of spreading control and GFP-VASP–expressing cells (Figure 8C).

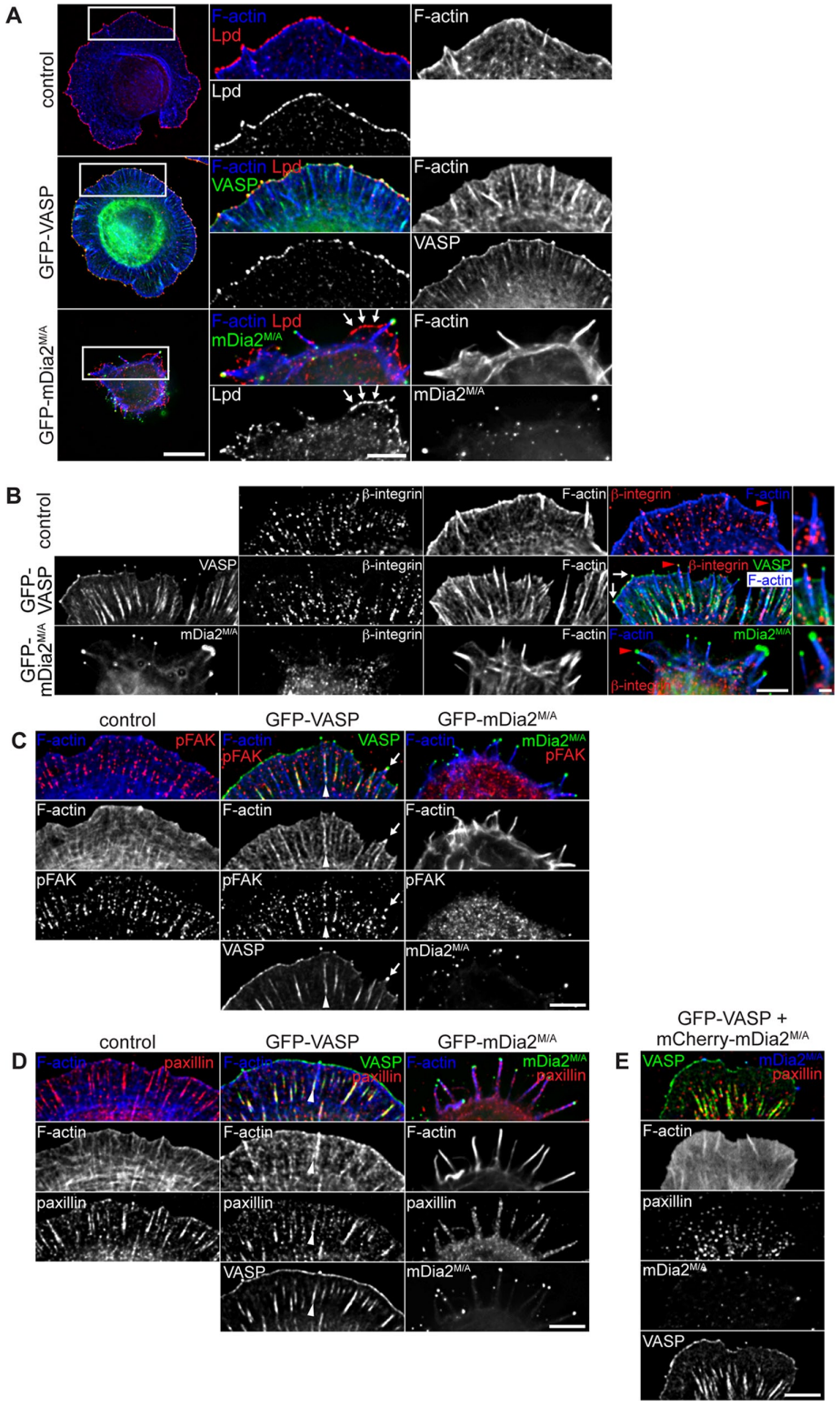

FIGURE 8: mDia2$^{M/A}$-initiated filopodia lack protrusive and adhesive structures. At 24 h posttransfection, MV^{D7} cells were allowed to spread on laminin for 30 min, fixed, and immunostained for (A) Lpd, (B) activated β1 integrin subunit, (C) activated FAK (pFAK), or (D) paxillin. (A) Lamellipodium formation in spreading GFP-mDia2$^{M/A}$–expressing cells is dramatically reduced (arrows). Right, magnification of boxed regions. (B) β1 integrin is not activated in tips of mDia2$^{M/A}$-containing filopodia. Activated β1 integrin colocalizes with GFP-VASP to filopodia tips (arrows). Red arrowheads indicate individual filopodia magnified on the right. (C) Activated FAK is not recruited to filopodia tips or focal adhesions in GFP-mDia2$^{M/A}$–expressing cells. In contrast, pFAK and GFP-VASP colocalize at filopodia tips (arrows) and in focal adhesions at the base of VASP-labeled filopodia (arrowheads). (D) Paxillin-containing focal adhesions are absent in spreading GFP-mDia2$^{M/A}$–expressing MV^{D7} cells but are formed at the base of VASP-labeled filopodia (arrowheads). (E) Formation of elongated paxillin-containing focal adhesions in spreading mDia2$^{M/A}$-expressing cells is rescued in the presence of VASP. All images are from at least two independent experiments. Scale bars, 10 μm; magnified images, 5 μm; magnified images of single filopodia in B, 1 μm.

Activation of Src, an immediate downstream signaling kinase of FAK (Schaller *et al.*, 1994; Lietha *et al.*, 2007), yielded comparable results (Supplemental Figure S9A). We thus hypothesize that activation of integrin-dependent signaling cascades needed for substrate attachment is compromised in GFP-mDia2$^{M/A}$–expressing cells, in turn impairing focal contact and adhesion formation during early spreading. Accordingly, the canonical focal adhesion markers vinculin and paxillin localized mostly diffusely to the cytoplasm in GFP-mDia2$^{M/A}$–expressing cells, with paxillin also localizing in a punctate pattern along the length of filopodia (Figure 8D and Supplemental Figure S9B). However, no focal adhesion–like staining of endogenous vinculin or paxillin was detectable in spreading GFP-mDia2$^{M/A}$–expressing MV^{D7} cells, indicating failure to support adhesion maturation. In contrast, these markers labeled elongated focal adhesions in spreading control and GFP-VASP cells (Figure 8D and Supplemental Figure S9B), showing that adhesions localized at the base of actin bundles in VASP-containing filopodia and microspikes. These findings suggest a role for VASP-assembled filopodia in initiating cellular attachment to the ECM through β1 integrin signaling (Nemethova *et al.*, 2008; Geiger *et al.*, 2009; Schäfer *et al.*, 2009). Accordingly, VASP rescued focal adhesion assembly in spreading cells coexpressing mDia2$^{M/A}$ (Figure 8E), indicating that VASP restores initiation of signaling pathways that regulate the formation of cell-matrix adhesions in the presence of mDia2$^{M/A}$.

Hence our data indicate that impaired spreading of MV^{D7} cells expressing GFP-mDia2$^{M/A}$ is caused by deficient activation of integrin-dependent signaling cascades, which results in a failure to form substrate adhesion at filopodium tips, assembly of nascent focal complexes, and maturation of focal adhesions in the lamellipodium. Of importance, these defects were rescued in cells simultaneously producing VASP, revealing a key role of this actin regulatory protein

in coordinating the various dynamic facets that result in the formation of competent filopodia.

DISCUSSION

The complex process of filopodia assembly requires the precise interplay and balance of key mechanistic components. Clearly, numerous molecules participate in filopodium formation; however, whether filopodia initiated by distinct molecular mechanisms are dynamically, structurally and functionally distinct is unresolved. The use of Ena/VASP- and mDia2-deficient MV^{D7} fibroblasts as a model system has enabled us to tease apart the individual contributions of VASP and mDia2 to filopodia assembly, structure, and function.

Filopodia formed via either VASP- or mDia2-driven mechanisms are substantially different, despite the presence of several hallmark molecules. In the absence of Ena/VASP, filopodia assembled by constitutively active mDia2$^{M/A}$ are 1.5-fold longer than in MV^{D7} control cells (Figure 1, B and D), probably because mDia2$^{M/A}$ promotes extensive actin filament elongation within filopodia, supports increased elongation rates, or is more refractory to capping that terminates filament elongation. In addition, ultrastructural analyses failed to detect filopodial actin filament bundles with splayed roots anchored in the lamellipodial cytoskeleton in GFP-mDia2$^{M/A}$–expressing cells (Figure 5 and Supplemental Figure S8), indicating that these filaments are unlikely to have formed by convergent elongation of actin filaments from a dendritic network but are likely generated by nucleation of linear F-actin filaments that rapidly elongate. While the manuscript of this article was under revision, Bilancia *et al*. (2014) published an elegant study combining in vitro and in vivo analyses to investigate the interplay between Dia and Ena, the sole *Drosophila* orthologues of mDia2 and Ena/VASP, respectively. Similar to our findings with VASP and mDia2$^{M/A}$, they demonstrated that expression of activated Dia (DiaΔDAD) resulted in filopodia that were significantly longer than those resulting from Ena expression in D16 cells. Furthermore, they found that elevated levels of Ena or activated DiaΔDAD resulted in increased numbers of filopodia with substantially different properties (Bilancia *et al.*, 2014). However, the *Drosophila* and mammalian systems showed strikingly different effects on filopodia stability, with DiaΔDAD-containing filopodia exhibiting an average lifetime of ~97 s versus an average of ~68 s for Ena-containing filopodia, whereas we observed the opposite trend, with mDia2$^{M/A}$ and VASP filopodia lifetimes of ~150 and ~250 s, respectively. The similarity in effects on length may be attributable to faster elongation rates and longer barbed-end residence times of DiaΔDAD and mDia2$^{M/A}$ compared with those of Ena and VASP. It is less clear why the trends in stability were reversed in the two systems, especially given the differences in cell type and experimental conditions. Thus, whereas both studies demonstrated clear differences in the behavior of filopodia containing either one or both types of actin regulator, the nature of the interplay differs in some respects, likely reflecting species- and paralogue-specific differences that, presumably, evolved to support greater regulatory and functional diversity of actin-driven protrusion in vertebrate systems. Consistent with this idea, the three vertebrate Ena/VASP proteins differ from one another and differ even more substantially from the DdVASP and *Drosophila* Ena proteins in their effects on F-actin elongation rates and the average times they associate with elongating barbed ends (Breitsprecher *et al.*, 2011; Winkelman *et al.*, 2014). It will be particularly interesting to examine adhesion pathways in the two model systems, given that the differential effects we observed between mDia2$^{M/A}$ and VASP on filopodia dynamics may arise from variations in integrin-mediated adhesion.

mDia2$^{M/A}$-generated filopodia displayed irregular dynamics, shorter lifetime, and diminished protrusive persistence, which appeared to substantially impair initial cell–matrix contact formation at their tips, a crucial step for integrin-dependent signaling events required for assembly of adhesion sites (Figure 4; DePasquale and Izzard, 1987; Rinnerthaler *et al.*, 1988; Partridge and Marcantonio, 2006). The Brownian ratchet model predicts that effective membrane protrusion requires optimal actin filament length to overcome bending rigidity, and filaments that exceed this length no longer sustain the external membrane force and collapse (Mogilner and Oster, 1996; Borisy and Svitkina, 2000; Pollard and Berro, 2009). Only filopodia of an ideal length can carry a maximal axial load without buckling ("Euler buckling length"). We propose that, without Ena/VASP, rapid mDia2-driven actin nucleation in filopodium tips, plus increased filament elongation rates and poor anchoring of filament bundles to the underlying cytoskeleton, results in long actin filaments that most likely exceed the Euler buckling length and fail to counteract membrane tension (Mogilner and Rubinstein, 2005).

We found that integrin-dependent signaling pathways that promote the assembly and maturation of cell–matrix contacts are deregulated at filopodia tips in GFP-mDia2$^{M/A}$–expressing MV^{D7} cells, resulting in impaired activation of the signaling-protein scaffolds FAK and Src, which coordinate cytoskeletal dynamics downstream of integrins (Figure 8 and Supplemental Figure S9; Parsons *et al.*, 2000; Arias-Salgado *et al.*, 2003). In particular, FAK regulates the assembly and maturation of focal adhesions (Mitra *et al.*, 2005), and mature focal adhesions are virtually absent in mDia2$^{M/A}$-expressing cells, except when VASP is coexpressed. The failure of GFP-mDia2$^{M/A}$–assembled filopodia to integrate signaling pathways at their tips may be intensified by their structural instability and erratic dynamics due to the absence of securely anchored filopodial actin bundles. We hypothesize that the observed adhesion defect in mDia2$^{M/A}$-expressing cells impedes the formation of protrusive structures like lamellipodia, thereby interfering with coordinated cell spreading (Figures 7 and 8).

Of importance, VASP compensates for the observed mDia2$^{M/A}$-driven phenotypes of increased filopodial length, low filopodia lifetime, low protrusive persistence of filopodia, diminished focal adhesion formation, and poor spreading (Figures 1D, 4, B and C, 7, and 8E). Thus, although VASP and mDia2$^{M/A}$ do not have to synergize for filopodia formation (Figure 1), VASP activity transforms filopodia that contain both proteins and makes them appear morphologically and dynamically more "VASP"-like by reducing their length and restoring lifetime, as well as their protrusive persistence (Figures 1D and 4, A–C). This VASP dominance suggests that additional, unknown factors are present in filopodia to support VASP-mediated actin dynamics and that these additional factors may be missing in experiments using purified proteins. We hypothesize that VASP activity is essential for initiating integrin-dependent matrix contacts at the filopodium tip, which triggers recruitment of signaling components to regulate maturation of focal adhesions, anchoring of actin stress fibers, and thus cell protrusion and spreading (Partridge and Marcantonio, 2006). Accordingly, VASP-containing filopodium tip "spots" initiate formation of nascent focal contacts (Figure 4, E–H, and Supplemental Figure S5; Schäfer *et al.*, 2009), whereas mDia2$^{M/A}$-generated filopodia cannot efficiently support formation of cell–matrix contacts without Ena/VASP (Figure 4, E–H). In addition, Ena/VASP is required for integrin-dependent endothelial barrier function in vivo (Furman *et al.*, 2007), and β-integrin–mediated adhesion is impaired in VASP-deficient endothelial cells (Schlegel and Waschke, 2009), suggesting direct correlation of VASP activity and integrin-mediated cell adhesion. We propose

that this VASP-integrin signaling contributes critically to restore filopodia tip adhesion in mDia2$^{M/A}$-expressing cells.

VASP activity may further improve stability of mDia2$^{M/A}$-generated filopodia by organizing actin filaments and controlling filopodial length. Ena/VASP regulates the F-actin architecture in fibroblast lamellipodia and neuronal growth cones by antagonizing CP and promoting formation of long, unbranched filaments (Bear *et al.*, 2002; Lebrand *et al.*, 2004). Filopodia containing VASP and mDia2$^{M/A}$ are shorter than those containing mDia2$^{M/A}$ alone, similar to filopodia containing only VASP (Figure 1D). VASP could control filopodia elongation by regulating mDia2-driven actin polymerization, either directly, by entering into a complex with mDia2, or indirectly, by modulating actin filament architecture at the filopodium tip to limit mDia2 processivity. Of note, *Drosophila* Ena also appears to dominate DiaΔDAD effects on filopodial behavior, presumably via negative regulation of Dia-mediated nucleation of linear F-actin filaments (Bilancia *et al.*, 2014). A direct interaction in vitro has been observed between the *Dictyostelium* and *Drosophila* Ena/VASP and mDia2 orthologues and for mammalian VASP with mDia1 and mDia2 (Grosse *et al.*, 2003; Schirenbeck *et al.*, 2006; Homem and Peifer, 2009; Figure 3, C–E). Given that the EVH1 domains of VASP and Ena mediate binding to the mDia2 FH2 domain and the Dia FH1 domain, respectively, it is possible that an inhibitory or other regulatory effect of EVH1 on Dia (Bilancia *et al.*, 2014) may be conserved in the mammalian system. In addition, it is also possible that VASP binding may trigger structural changes in mDia2 to slow processive filament elongation, possibly by inducing mDia2's self-inhibitory conformation. Alternatively, VASP could limit access of mDia2 to barbed ends by partially overlapping with mDia2's binding site on the barbed end or changing the conformation of barbed ends upon filament clustering (Applewhite *et al.*, 2007). A key function of tip-associated VASP may be to tether filaments to the cell periphery (Breitsprecher *et al.*, 2008; Faix *et al.*, 2009), in essence as a stabilizing linker between filament barbed ends and the cell membrane to enable efficient membrane tip protrusion. In agreement with this, Cdc42-dependent activation of IRSp53 was shown to cluster VASP at the plasma membrane to promote filopodia initiation (Disanza *et al.*, 2013).

Intriguingly, the majority of mDia2$^{M/A}$-assembled filopodia contain microtubules that increase filopodia length (Figure 6). Such engagement of dynamic microtubules with actin bundles is commonly observed in filopodia of neuronal growth cones and contributes to filopodia formation, neuritogenesis, and growth cone turning (Challacombe *et al.*, 1996; Williamson *et al.*, 1996; Dent *et al.*, 2007). In contrast, microtubule exploration of filopodia in nonneuronal cells is uncommon, and no reports exist of microtubules reaching into filopodium tips of fibroblasts. mDia2 coordinates actin and microtubule dynamics, associates processively with barbed ends, and also binds and stabilizes microtubules (Palazzo *et al.*, 2001; Wen *et al.*, 2004; Bartolini *et al.*, 2008; Chesarone *et al.*, 2010). Thus mDia2 could promote microtubule exploration of filopodia by linking dynamic microtubule ends to rapidly polymerizing barbed ends of actin filaments. Accordingly, dynamic microtubules and F-actin colocalize with mDia2$^{M/A}$ at filopodium tips (Figure 6A and Supplemental Figure S6); however, microtubules are not required to generate or maintain mDia2$^{M/A}$-dependent filopodia (Figure 6, C–E). Given their higher resistance to bending forces (i.e., high flexural rigidity) compared with actin filaments (Gittes *et al.*, 1993), microtubules may increase actin bundle stiffness in mDia2$^{M/A}$-generated filopodia, thereby overcoming the external membrane force at the filopodium tip and allowing continuous filament protrusion. The reduced length of mDia2$^{M/A}$-assembled filopodia after microtubule depolymerization supports this possibility (Figure 6F).

Collectively our data underscore that excessive filament elongation generates filopodia that do not support persistent membrane protrusion. This effect may be intensified in filopodial actin bundles that are insufficiently connected to the underlying lamellipodial cytoskeleton (Figure 5 and Supplemental Figure S8). Moreover, signaling cascades initiated at filopodia tips are critical for proper attachment and effective protrusion of motile cells. Of importance, filopodia assembled by distinct molecular pathways do not facilitate these processes equally: in particular, VASP-containing filopodia efficiently support surface probing, integrin activation, attachment, membrane protrusion, and early cell spreading, whereas mDia2$^{M/A}$-initiated filopodia fail to initiate these processes without Ena/VASP. Whereas synergy between VASP activity and mDia2$^{M/A}$ is not required for filopodium formation as proposed (Schirenbeck *et al.*, 2005a), VASP activity alters key properties of mDia2$^{M/A}$-containing filopodia, enabling the initial focal contact formation and integrin-dependent signaling processes required for proper cell attachment, membrane protrusion, and subsequent cell area expansion. We propose that along with opposing CP and clustering barbed ends at filopodium tips, VASP initiates integrin-dependent cell–matrix contacts at the filopodium tip and assists in molecular processes that provide stability for mDia2-nucleated filopodium bundles. Future analyses will need to determine the molecular mechanism underlying mDia2 regulation by VASP and how the lack of VASP might negatively affect cell homeostasis.

MATERIALS AND METHODS

Expression plasmids, reagents, and antibodies

Subcloning and PCR were performed using standard methods. Full-length cDNAs for mouse *mdia2* and constitutively active *mdia2*$^{M/A}$ were gifts from A. Alberts (Van Andel Research Institute, Grand Rapids, MI) and were subcloned into pEGFP-C1 vectors (Clontech, Mountain View, CA) in frame with enhanced GFP (EGFP) or mCherry. Vectors for expression of GST fusion proteins of mDia2 FH2 domain (amino acid residues 614–1056) in *Escherichia coli* were generated by subcloning PCR fragments into pGEX-6P-1 (GE Healthcare, Piscataway, NJ). mDia2 FH2 mutant (FH2-F918D) was generated using the QuikChange Site-Directed Mutagenesis Kit (Agilent Technologies, Santa Clara, CA). The expression construct for His_6-VASP has been described (Barzik *et al.*, 2005). VASP ΔEVH1 (amino acid residues 113–376) was PCR amplified from mouse *vasp* cDNA and subcloned into pQE80 vector (Qiagen, Valencia, CA). pC2-EGFP vector containing bovine *myoX* cDNA was a gift from R. Cheney (University of North Carolina, Chapel Hill, NC). pEFmEGFP mDia2 DAD vector was a gift from G. Gundersen (Columbia University, New York, NY) and has been described (Alberts, 2001). pEGFP-C2 Rif vector was a gift from H. Mellor (University of Bristol, Bristol, United Kingdom). pCAGGS/ES-EGFP vectors containing cDNA for full-length mouse mDia1 and constitutively active mDia1ΔN3, respectively, were gifts from F. Wang (Duke University, Durham, NC). pmCherry-N1 EB1 vector was a gift from T. Wittmann and C. Waterman (National Institutes of Health, Bethesda, MD). Vectors for EGFP-tagged N-WASP-CA (Strasser *et al.*, 2004) and mCherry-tagged β-actin (Dent *et al.*, 2007) are described elsewhere.

Unless noted, all reagents were purchased from Sigma-Aldrich (St. Louis, MO).

Rabbit anti-mDia antibodies were gifts from A. Alberts and were used at 1:5000 (mDia1, mDia2) or 1:2000 (mDia3), respectively. Rabbit-anti-VASP antibody 2010 (Bear *et al.*, 2002) was used at 1:10,000 in Western blots. Rabbit-anti-Mena antibody 2197 (1:500; Bear *et al.*, 2000) was used to label Ena/VASP proteins in cells, since this antibody resulted in more robust detection of endogenous proteins

compared with the VASP antibody, in particular in the FP4-mito recruitment experiments. Mouse anti–α-tubulin at 1:4000 (DM1A), rat anti–tyrosinated tubulin at 1:1000 (YL1/2; Millipore, Burlington, MA), and rabbit anti–detyrosinated tubulin at 1:500 (Millipore) were used to label microtubules. Mouse anti–α-tubulin antibody DM1A was used at 1:40,000 to detect tubulin in Western blots. Immunostaining for fascin was performed by methanol fixation of cells at –20°C and then using mouse anti-human fascin (55K-2; DakoCytomation, Fort Collins, CO) at 1:50. All other antibodies were used as follows: affinity-purified rabbit anti-Lpd, 1:400 (Krause *et al*., 2004); mouse anti–phospho-tyrosine antibody (4G10), 1:400 (Millipore); chicken anti-MyoX antibody (a gift from R. Cheney), 1:500; rat anti–activated β1 integrin (CD29; clone 9EG7; BD Transduction Laboratories, San Jose, CA), 1:50; mouse anti-paxillin (BD Transduction Laboratories), 1:200; mouse anti-vinculin, 1:400; rabbit anti–phospho-Src family (Tyr-416; Cell Signaling Technology, Danvers, MA), 1:400; and mouse-anti human pY397 FAK (BD Transduction Laboratories), 1:100. Alexa-conjugated secondary antibodies and Alexa-conjugated phalloidin were purchased from Invitrogen (Carlsbad, CA) and used at 1:250–1:1000. Phalloidin conjugated to Alexa 350, Alexa 488, Alexa 594, or Alexa 647 was used to label F-actin.

Recombinant protein expression and purification

The (His_6)-tagged VASP and VASP ΔEVH1 proteins were purified as described (Barzik *et al*., 2005). GST, recombinant GST-tagged mDia2 FH2 domain (amino acids 615–1013), and GST-FH2-F918D were expressed in *E. coli* BL21-CodonPlus(DE3)-RP strain (Agilent Technologies) and purified by chromatography on glutathione Sepharose (GS) resin (GE Healthcare) in phosphate-buffered saline (PBS) buffer plus 2 mM β-mercaptoethanol.

Assay for binding of purified proteins

For GST pull-down assays, purified His_6-VASP proteins were incubated with 50 μg of GST or GST-FH2 domain, immobilized on GS for 1 h at 4°C in binding buffer (PBS, 2% bovine serum albumin, 2 mM β-mercaptoethanol, and protease inhibitor cocktail [Complete Mini; Roche Applied Sciences, Indianapolis, IN]). GS was washed twice with binding buffer and twice with binding buffer plus 1 M NaCl. Proteins were eluted with 2× Laemmli sample buffer and subjected to SDS–PAGE and Western blot analysis.

Cell and cortical neuron culture and transfection

MV^{D7} cells were cultured as described (Bear *et al*., 2000). MV^{D7} EGFP-VASP cells are stable cell lines that have been described, and MV^{D7} RFP-VASP cells were generated using the same methodology (Loureiro *et al*., 2002). For platinum-replica electron microscopy experiments, stable MV^{D7} EGFP-$mDia2^{M/A}$ cells were generated as described (Loureiro *et al*., 2002). For all other experiments, MV^{D7} cells were transiently transfected with mDia2 or the expression constructs indicated using Amaxa Nucleofector technology, using cell nucleofection solution MEF-2 and program A-23, according to the manufacturer's recommendations (Lonza, Cologne, Germany). Transfected cells were incubated at 32°C for 24–36 h before further experimentation. For immunofluorescence analysis, cells were plated on acid-washed coverslips coated with fibronectin (10 μg/ml). For live-cell imaging, cells were plated on fibronectin-coated glass-bottom dishes (MatTek, Ashland, MA).

NIH3T3 cells and wild-type MEFs were cultured in DME supplemented with 10% fetal bovine serum and maintained at 37°C, 5% CO_2. Cortical neuron cultures were prepared from embryonic day (E) 15.5 mice and transfected as described (Dent *et al*., 2007).

Immunocytochemistry

Unless otherwise noted, cells were fixed with 4% (wt/vol) paraformaldehyde (PFA) in PHEM buffer (60 mM 1,4-piperazinediethanesulfonic acid, pH 7.0, 25 mM 4-(2-hydroxyethyl)-1-piperazineethanesulfonic acid, pH 7.0, 10 mM ethylene glycol tetraacetic acid, 2 mM $MgCl_2$, 0.12 M sucrose) for 15 min at room temperature and permeabilized with 0.1% (vol/vol) Triton X-100 in TBS (50 mM Tris/HCl, pH 7.4, 150 mM NaCl) for 2 min at room temperature. Coverslips were rinsed in TBS and labeled with primary antibody in 10% serum in TBS for 1 h at room temperature. Coverslips were washed twice with TBS and incubated with fluorophore-conjugated secondary antibody and/or phalloidin for 1 h at room temperature. Coverslips were washed and mounted on glass slides using Fluoromount-G (Electron Microscopy Sciences, Hatfield, PA). For certain experiments, cells were fixed in –20°C methanol, omitting the permeabilization step.

Image analysis and quantification

Live or fixed cells were imaged on a DeltaVision deconvolution microscopy system (Applied Precision, Issaquah, WA) consisting of a CoolSnap camera attached to an Olympus IX71 microscope equipped with a mercury light source; a 40×/numerical aperture (NA) 1.0 Plan Apo or a 60×/NA 1.4 Plan Apo Nikon objective lens was used, depending on the experiment. During time-lapse microscopy, cells were incubated at 32°C in 5% CO_2 (Solent, Segensworth, United Kingdom). Nocodazole treatment was performed by exchanging half of the culture media with prewarmed drug-containing culture media to yield a concentration of 100 ng/ml nocodazole.

All images were collected and processed using softWoRx software (SGI, Mountain View, CA) and compiled using Photoshop (Adobe, San Jose, CA). Further image analysis was performed using MetaMorph software (Molecular Devices, Sunnyvale, CA).

Filopodia quantification. VASP or $mDia2^{M/A}$ tip localization was used to identify and count filopodia manually using the Region Measurements function in MetaMorph software. Immunostaining for Lpd was used to identify filopodia in control and GFP-mDia2–expressing cells. Filopodia length was determined by tracing filopodia from their tip to the base (cell edge) in images of cells labeled with phalloidin using either the line or the polyline tool in MetaMorph software.

For measurement of Lpd-labeled leading edge, cells were transfected as indicated, stained with antibody against Lpd, and F-actin was labeled with phalloidin. The cell perimeter was traced manually in MetaMorph software, and total circumference was calculated using the Region Measurement function. Next, the Lpd-positive fraction of the cell perimeter was identified and traced. Only continuous Lpd signal for at least 20 pixels (2.158 μm) was used for data analysis. The sum of Lpd-positive distance along the cell edge was divided by the total cell circumference to yield the percentage of Lpd-labeled cell edge.

To quantify protrusive persistence of filopodia, individual GFP-VASP– or GFP-$mDia2^{M/A}$–labeled filopodium tips, or filopodial tips colabeled with mCherry-VASP and GFP-$mDia2^{M/A}$, were tracked in frames of live-cell image acquisitions using the Track Objects application in MetaMorph software. Owing to irregular dynamics of GFP-$mDia2^{M/A}$ filopodia, filopodium tips were tracked manually in most frames. Individual frames in which GFP-$mDia2^{M/A}$–labeled filopodium tips went out of focus were omitted from quantification. Change in directionality (Δx, Δy) and straight-line distance from start to finish points (d) traveled by the filopodium tip was measured. The following formula was used to calculate protrusive persistence:

$$\text{Protrusive persistence} = \frac{d}{\sum_n \sqrt{(\Delta x_n)^2 + (\Delta y_n)^2}}$$

Quantification of zyxin-labeled focal adhesions associated with filopodia. Zyxin-labeled focal adhesions were considered to be associated with a filopodium if they 1) assembled at the base of an actively protruding filopodium in live-cell imaging experiments and had a lifetime of at least three frames (=15 s) and/or 2) were clearly detectable in the shaft of the filopodium.

Measurement of average cell area. Cells were transfected as indicated and chemically fixed, and F-actin was labeled with phalloidin. For each cell, the cell perimeter was traced manually (using the signal from phalloidin-labeled F-actin), and area was calculated using MetaMorph software.

Cell spreading assay

MV^{D7} cells were transfected with pEGFP-mDia2$^{M/A}$ vector, using the Amaxa nucleofection technique. Twenty-four hours posttransfection, transiently transfected cells, control MV^{D7} cells, and MV^{D7} cells stably expressing GFP-VASP were trypsinized, allowed to recover in medium suspension for 20–30 min, and replated on laminin-coated coverslips (20 µg/ml). Cells were allowed to spread for 30 min and fixed carefully with 4 % PFA in PHEM buffer for 15 min at room temperature. Coverslips were then gently processed as described.

Platinum-replica electron microscopy

Platinum-replica electron microscopy was performed as described (Bear *et al.*, 2002) on nontransfected MV^{D7} control cells and MV^{D7} cells stably expressing GFP-VASP or GFP-mDia2$^{M/A}$.

Immunoblotting

Protein lysates were prepared as described (Kovacs *et al.*, 2006). SDS–PAGE and immunoblot analyses were performed using standard procedures with horseradish peroxidase–conjugated secondary antibodies at 1:40,000. Signal was detected using the Amersham ECL Prime Western Blotting Detection Reagent (GE Healthcare, Pittsburgh, PA).

Statistical analysis

All statistical tests were performed with Prism 5.0c software (GraphPad, La Jolla, CA). For each data set, the Shapiro–Wilk normality test was performed to determine Gaussian distribution. Parametric or nonparametric statistical tests and post hoc tests were performed, depending on the variance of the data sets. Statistical differences between two conditions were determined by Student's *t* test. For multiple conditions, means were compared by analysis of variance. All data found to be significant ($p < 0.05$) by analysis of variance were compared with either Tukey's honestly significant difference or Bonferroni–Dunn's post hoc test to reveal statistically different groups. For all statistical analyses, the mean values ± SEM are given, unless indicated otherwise.

ACKNOWLEDGMENTS

We thank M. Machner, N. Rusan, and J. Bird for critical reading of the manuscript. We are grateful to K. Remmert for providing wild-type MEFs. F.B.G. was supported by National Institutes of Health Grant GM58801 and Integrated Cancer Biology Program Grant 1-U54-CA112967. S.L.G. was supported by National Institutes of Health Grant R01GM108970. This work was also supported by National Institutes of Health intramural funds from the National Institute on Deafness and Other Communication Disorders (NIDCD) 1 Z01 DC000039-17 to T. Friedman (Laboratory of Molecular Genetics, NIDCD, National Institutes of Health).

REFERENCES

Alberts AS (2001). Identification of a carboxyl-terminal diaphanous-related formin homology protein autoregulatory domain. J Biol Chem 276, 2824–2830.

Alexandrova AY, Arnold K, Schaub S, Vasiliev JM, Meister JJ, Bershadsky AD, Verkhovsky AB (2008). Comparative dynamics of retrograde actin flow and focal adhesions: formation of nascent adhesions triggers transition from fast to slow flow. PloS One 3, e3234.

Applewhite DA, Barzik M, Kojima S, Svitkina TM, Gertler FB, Borisy GG (2007). Ena/VASP proteins have an anti-capping independent function in filopodia formation. Mol Biol Cell 18, 2579–2591.

Arias-Salgado EG, Lizano S, Sarkar S, Brugge JS, Ginsberg MH, Shattil SJ (2003). Src kinase activation by direct interaction with the integrin beta cytoplasmic domain. Proc Natl Acad Sci USA 100, 13298–13302.

Aspenström P (2010). Formin-binding proteins: modulators of formin-dependent actin polymerization. Biochim Biophys Acta 1803, 174–182.

Ball LJ, Kuhne R, Hoffmann B, Hafner A, Schmieder P, Volkmer-Engert R, Hof M, Wahl M, Schneider-Mergener J, Walter U, *et al.* (2000). Dual epitope recognition by the VASP EVH1 domain modulates polyproline ligand specificity and binding affinity. EMBO J 19, 4903–4914.

Bartolini F, Moseley JB, Schmoranzer J, Cassimeris L, Goode BL, Gundersen GG (2008). The formin mDia2 stabilizes microtubules independently of its actin nucleation activity. J Cell Biol 181, 523–536.

Barzik M, Kotova TI, Higgs HN, Hazelwood L, Hanein D, Gertler FB, Schafer DA (2005). Ena/VASP proteins enhance actin polymerization in the presence of barbed end capping proteins. J Biol Chem 280, 28653–28662.

Bear JE, Loureiro JJ, Libova I, Fässler R, Wehland J, Gertler FB (2000). Negative regulation of fibroblast motility by Ena/VASP proteins. Cell 101, 717–728.

Bear JE, Svitkina TM, Krause M, Schafer DA, Loureiro JJ, Strasser GA, Maly IV, Chaga OY, Cooper JA, Borisy GG, *et al.* (2002). Antagonism between Ena/VASP proteins and actin filament capping regulates fibroblast motility. Cell 109, 509–521.

Beli P, Mascheroni D, Xu D, Innocenti M (2008). WAVE and Arp2/3 jointly inhibit filopodium formation by entering into a complex with mDia2. Nat Cell Biol 10, 849–857.

Bilancia CG, Winkelman JD, Tsygankov D, Nowotarski SH, Sees JA, Comber K, Evans I, Lakhani V, Wood W, Elston TC, *et al.* (2014). Enabled negatively regulates diaphanous-driven actin dynamics in vitro and in vivo. Dev Cell 28, 394–408.

Block J, Stradal TEB, Hänisch J, Geffers R, Köstler SA, Urban E, Small JV, Rottner K, Faix J (2008). Filopodia formation induced by active mDia2/Drf3. J Microsc 231, 506–517.

Bohil AB, Robertson BW, Cheney RE (2006). Myosin-X is a molecular motor that functions in filopodia formation. Proc Natl Acad Sci USA 103, 12411–12416.

Borisy GG, Svitkina TM (2000). Actin machinery: pushing the envelope. Curr Opin Cell Biol 12, 104–112.

Breitsprecher D, Kiesewetter AK, Linkner J, Urbanke C, Resch GP, Small JV, Faix J (2008). Clustering of VASP actively drives processive, WH2 domain-mediated actin filament elongation. EMBO J 27, 2943–2954.

Breitsprecher D, Kiesewetter AK, Linkner J, Vinzenz M, Stradal TE, Small JV, Curth U, Dickinson RB, Faix J (2011). Molecular mechanism of Ena/VASP-mediated actin-filament elongation. EMBO J 30, 456–467.

Burnette DT, Manley S, Sengupta P, Sougrat R, Davidson MW, Kachar B, Lippincott-Schwartz J (2011). A role for actin arcs in the leading-edge advance of migrating cells. Nat Cell Biol 13, 371–381.

Campellone KG, Welch MD (2010). A nucleator arms race: cellular control of actin assembly. Nat Rev Mol Cell Biol 11, 237–251.

Carl UD, Pollmann M, Orr E, Gertlere FB, Chakraborty T, Wehland J (1999). Aromatic and basic residues within the EVH1 domain of VASP specify its interaction with proline-rich ligands. Curr Biol 9, 715–718.

Challacombe JF, Snow DM, Letourneau PC (1996). Actin filament bundles are required for microtubule reorientation during growth cone turning to avoid an inhibitory guidance cue. J Cell Sci 109, 2031–2040.

Chesarone MA, DuPage AG, Goode BL (2010). Unleashing formins to remodel the actin and microtubule cytoskeletons. Nat Rev Mol Cell Biol 11, 62–74.

Chhabra ES, Higgs HN (2007). The many faces of actin: matching assembly factors with cellular structures. Nat Cell Biol 9, 1110–1121.

Davenport RW, Dou P, Rehder V, Kater SB (1993). A sensory role for neuronal growth cone filopodia. Nature 361, 721–724.
Dent EW, Kwiatkowski AV, Mebane LM, Philippar U, Barzik M, Rubinson DA, Gupton S, Van Veen JE, Furman C, Zhang J, *et al.* (2007). Filopodia are required for cortical neurite initiation. Nat Cell Biol 9, 1347–1359.
DePasquale JA, Izzard CS (1987). Evidence for an actin-containing cytoplasmic precursor of the focal contact and the timing of incorporation of vinculin at the focal contact. J Cell Biol 105, 2803–2809.
Disanza A, Bisi S, Winterhoff M, Milanesi F, Ushakov DS, Kast D, Marighetti P, Romet-Lemonne G, Muller HM, Nickel W, *et al.* (2013). CDC42 switches IRSp53 from inhibition of actin growth to elongation by clustering of VASP. EMBO J 32, 2735–2750.
Faix J, Breitsprecher D, Stradal TE, Rottner K (2009). Filopodia: complex models for simple rods. Int J Biochem Cell Biol 41, 1656–1664.
Furman C, Sieminski AL, Kwiatkowski AV, Rubinson DA, Vasile E, Bronson RT, Fassler R, Gertler FB (2007). Ena/VASP is required for endothelial barrier function in vivo. J Cell Biol 179, 761–775.
Galbraith CG, Yamada KM, Galbraith JA (2007). Polymerizing actin fibers position integrins primed to probe for adhesion sites. Science 315, 992–995.
Gates J, Mahaffey JP, Rogers SL, Emerson M, Rogers EM, Sottile SL, Van Vactor D, Gertler FB, Peifer M (2007). Enabled plays key roles in embryonic epithelial morphogenesis in *Drosophila*. Development 134, 2027–2039.
Geiger B, Spatz JP, Bershadsky AD (2009). Environmental sensing through focal adhesions. Nat Rev Mol Cell Biol 10, 21–33.
Gittes F, Mickey B, Nettleton J, Howard J (1993). Flexural rigidity of microtubules and actin filaments measured from thermal fluctuations in shape. J Cell Biol 120, 923–934.
Goode BL, Eck MJ (2007). Mechanism and function of formins in the control of actin assembly. Annu Rev Biochem 76, 593–627.
Grosse R, Copeland JW, Newsome TP, Way M, Treisman R (2003). A role for VASP in RhoA-Diaphanous signalling to actin dynamics and SRF activity. EMBO J 22, 3050–3061.
Guillou H, Depraz-Depland A, Planus E, Vianay B, Chaussy J, Grichine A, Albiges-Rizo C, Block MR (2008). Lamellipodia nucleation by filopodia depends on integrin occupancy and downstream Rac1 signaling. Exp Cell Res 314, 478–488.
Han YH, Chung CY, Wessels D, Stephens S, Titus MA, Soll DR, Firtel RA (2002). Requirement of a vasodilator-stimulated phosphoprotein family member for cell adhesion, the formation of filopodia, and chemotaxis in dictyostelium. J Biol Chem 277, 49877–49887.
Hansen SD, Mullins RD (2010). VASP is a processive actin polymerase that requires monomeric actin for barbed end association. J Cell Biol 191, 571–584.
Higgs HN (2005). Formin proteins: a domain-based approach. Trends Biochem Sci 30, 342–353.
Homem CC, Peifer M (2009). Exploring the roles of diaphanous and enabled activity in shaping the balance between filopodia and lamellipodia. Mol Biol Cell 20, 5138–5155.
Hufner K, Higgs HN, Pollard TD, Jacobi C, Aepfelbacher M, Linder S (2001). The verprolin-like central (vc) region of Wiskott-Aldrich syndrome protein induces Arp2/3 complex-dependent actin nucleation. J Biol Chem 276, 35761–35767.
Huttenlocher A, Ginsberg MH, Horwitz AF (1996). Modulation of cell migration by integrin-mediated cytoskeletal linkages and ligand-binding affinity. J Cell Biol 134, 1551–1562.
Hynes RO (2002). Integrins: bidirectional, allosteric signaling machines. Cell 110, 673–687.
Hüttelmaier S, Harbeck B, Steffens NO, Meßerschmidt T, Illenberger S, Jokusch BM (1999). Characterization of the actin binding properties of the vasodilator-stimulated phosphoprotein VASP. FEBS Lett 451, 68–74.
Katz BZ, Miyamoto S, Teramoto H, Zohar M, Krylov D, Vinson C, Gutkind JS, Yamada KM (2002). Direct transmembrane clustering and cytoplasmic dimerization of focal adhesion kinase initiates its tyrosine phosphorylation. Biochim Biophys Acta 1592, 141–152.
Kovacs EM, Makar RS, Gertler FB (2006). Tuba stimulates intracellular N-WASP-dependent actin assembly. J Cell Sci 119, 2715–2726.
Kovar DR, Harris ES, Mahaffy R, Higgs HN, Pollard TD (2006). Control of the assembly of ATP- and ADP-actin by formins and profilin. Cell 124, 423–435.
Kovar DR, Pollard TD (2004). Insertional assembly of actin filament barbed ends in association with formins produces piconewton forces. Proc Natl Acad Sci USA 101, 14725–14730.
Krause M, Leslie JD, Stewart M, Lafuente EM, Valderrama F, Jagannathan R, Strasser GA, Rubinson DA, Liu H, Way M, *et al.* (2004). Lamellipodin, an Ena/VASP ligand, is implicated in the regulation of lamellipodial dynamics. Dev Cell 7, 571–583.
Kureishy N, Sapountzi V, Prag S, Anilkumar N, Adams JC (2002). Fascins, and their roles in cell structure and function. Bioessays 24, 350–361.
Lauffenburger DA, Horwitz AF (1996). Cell migration: a physically integrated molecular process. Cell 84, 359–369.
Lebrand C, Dent EW, Strasser GA, Lanier LM, Krause M, Svitkina TM, Borisy GG, Gertler FB (2004). Critical role of Ena/VASP proteins for filopodia formation in neurons and in function downstream of netrin-1. Neuron 42, 37–49.
Li F, Higgs HN (2003). The mouse formin mDia1 is a potent actin nucleation factor regulated by autoinhibition. Curr Biol 13, 1335–1340.
Li F, Higgs HN (2005). Dissecting requirements for auto-inhibition of actin nucleation by the formin, mDia1. J Biol Chem 280, 6986–6992.
Lietha D, Cai X, Ceccarelli DF, Li Y, Schaller MD, Eck MJ (2007). Structural basis for the autoinhibition of focal adhesion kinase. Cell 129, 1177–1187.
Loureiro JJ, Rubinson DA, Bear JE, Baltus GA, Kwiatkowski AV, Gertler FB (2002). Critical roles of phosphorylation and actin binding motifs, but not the central proline-rich region, for Ena/vasodilator-stimulated phosphoprotein (VASP) function during cell migration. Mol Biol Cell 13, 2533–2546.
Mallavarapu A, Mitchison T (1999). Regulated actin cytoskeleton assembly at filopodium tips controls their extension and retraction. J Cell Biol 146, 1097–1106.
Mejillano MR, Kojima S, Applewhite DA, Gertler FB, Svitkina TM, Borisy GG (2004). Lamellipodial versus filopodial mode of the actin nanomachinery: pivotal role of the filament barbed end. Cell 118, 363–373.
Mitra SK, Hanson DA, Schlaepfer DD (2005). Focal adhesion kinase: in command and control of cell motility. Nat Rev Mol Cell Biol 6, 56–68.
Mogilner A, Oster G (1996). Cell motility driven by actin polymerization. Biophys J 71, 3030–3045.
Mogilner A, Rubinstein B (2005). The physics of filopodial protrusion. Biophys J 89, 782–795.
Moseley JB, Sagot I, Manning AL, Xu Y, Eck MJ, Pellman D, Goode BL (2004). A conserved mechanism for Bni1- and mDia1-induced actin assembly and dual regulation of Bni1 by Bud6 and profilin. Mol Biol Cell 15, 896–907.
Nemethova M, Auinger S, Small JV (2008). Building the actin cytoskeleton: filopodia contribute to the construction of contractile bundles in the lamella. J Cell Biol 180, 1233–1244.
Niebuhr K, Ebel F, Frank R, Reinhard M, Domann E, Carl UD, Walter U, Gertler FB, Wehland J, Chakraborty T (1997). A novel proline-rich motif present in ActA of *Listeria monocytogenes* and cytoskeletal proteins is the ligand for the EVH1 domain, a protein module present in the Ena/VASP family. EMBO J 16, 5433–5444.
Palazzo AF, Cook TA, Alberts AS, Gundersen GG (2001). mDia mediates Rho-regulated formation and orientation of stable microtubules. Nat Cell Biol 3, 723–729.
Parsons JT (2003). Focal adhesion kinase: the first ten years. J Cell Sci 116, 1409–1416.
Parsons JT, Horwitz AR, Schwartz MA (2010). Cell adhesion: integrating cytoskeletal dynamics and cellular tension. Nat Rev Mol Cell Biol 11, 633–643.
Parsons JT, Martin KH, Slack JK, Taylor JM, Weed SA (2000). Focal adhesion kinase: a regulator of focal adhesion dynamics and cell movement. Oncogene 19, 5606–5613.
Partridge MA, Marcantonio EE (2006). Initiation of attachment and generation of mature focal adhesions by integrin-containing filopodia in cell spreading. Mol Biol Cell 17, 4237–4248.
Pasic L, Kotova T, Schafer DA (2008). Ena/VASP proteins capture actin filament barbed ends. J Biol Chem 283, 9814–9819.
Paul AS, Pollard TD (2009). Review of the mechanism of processive actin filament elongation by formins. Cell Motil Cytoskeleton 66, 606–617.
Pellegrin S, Mellor H (2005). The Rho family GTPase Rif induces filopodia through mDia2. Curr Biol 15, 129–133.
Peng J, Wallar BJ, Flanders A, Swiatek PJ, Alberts AS (2003). Disruption of the Diaphanous-related formin Drf1 gene encoding mDia1 reveals a role for Drf3 as an effector for Cdc42. Curr Biol 13, 534–545.
Pistor S, Gröbe L, Sechi AS, Domann E, Gerstel B, Machesky LM, Chakraborty T, Wehland J (2000). Mutations of arginine residues within the 146-KKRRK-150 motif of the ActA protein of *Listeria monocytogenes* abolish intracellular motility by interfering with the recruitment of the Arp2/3 complex. J Cell Sci 113, 3277–3287.

Pollard TD, Berro J (2009). Mathematical models and simulations of cellular processes based on actin filaments. J Biol Chem 284, 5433–5437.
Pollard TD, Borisy GG (2003). Cellular motility driven by assembly and disassembly of actin filaments. Cell 112, 453–465.
Pruyne D, Evangelista M, Yang C, Bi E, Zigmond S, Bretscher A, Boone C (2002). Role of formins in actin assembly: nucleation and barbed-end association. Science 297, 612–615.
Rinnerthaler G, Geiger B, Small JV (1988). Contact formation during fibroblast locomotion: involvement of membrane ruffles and microtubules. J Cell Biol 106, 747–760.
Rohatgi R, Ma L, Miki H, Lopez M, Kirchhausen T, Takenawa T, Kirschner MW (1999). The Interaction between N-WASP and the Arp2/3 complex links Cdc42-dependent signals to actin assembly. Cell 97, 221–231.
Schäfer C, Borm B, Born S, Möhl C, Eibl EM, Hoffmann B (2009). One step ahead: role of filopodia in adhesion formation during cell migration of keratinocytes. Exp Cell Res 315, 1212–1224.
Schäfer C, Born S, Möhl C, Houben S, Kirchgeßner N, Merkel R, Hoffmann B (2010). The key feature for early migratory processes: dependence of adhesion, actin bundles, force generation and transmission on filopodia. Cell Adh Migr 4, 215–225.
Schaller MD, Hildebrand JD, Shannon JD, Fox JW, Vines RR, Parsons JT (1994). Autophosphorylation of the focal adhesion kinase, pp125FAK, directs SH2-dependent binding of pp60src. Mol Cell Biol 14, 1680–1688.
Schiller HB, Fässler R (2013). Mechanosensitivity and compositional dynamics of cell-matrix adhesions. EMBO Rep 14, 509–519.
Schirenbeck A, Arasada R, Bretschneider T, Schleicher M, Faix J (2005a). Formins and VASPs may co-operate in the formation of filopodia. Biochem Soc Trans 33, 1256–1259.
Schirenbeck A, Arasada R, Bretschneider T, Stradal TE, Schleicher M, Faix J (2006). The bundling activity of vasodilator-stimulated phosphoprotein is required for filopodium formation. Proc Natl Acad Sci USA 103, 7694–7699.
Schirenbeck A, Bretschneider T, Arasada R, Schleicher M, Faix J (2005b). The Diaphanous-related formin dDia2 is required for the formation and maintenance of filopodia. Nat Cell Biol 7, 619–625.
Schlegel N, Waschke J (2009). Impaired integrin-mediated adhesion contributes to reduced barrier properties in VASP-deficient microvascular endothelium. J Cell Phys 220, 357–366.
Shi Q, Boettiger D (2003). A novel mode for integrin-mediated signaling: tethering is required for phosphorylation of FAK Y397. Mol Biol Cell 14, 4306–4315.
Skoble J, Auerbuch V, Goley ED, Welch MD, Portnoy DA (2001). Pivotal role of VASP in Arp2/3 complex-mediated actin nucleation, actin branch-formation, and Listeria monocytogenes motility. J Cell Biol 155, 89–100.
Small JV, Stradal T, Vignal E, Rottner K (2002). The lamellipodium: where motility begins. Trends Cell Biol 12, 112–120.
Steketee M, Balazovich K, Tosney KW (2001). Filopodial initiation and a novel filament-organizing center, the focal ring. Mol Biol Cell 12, 2378–2395.
Strasser GA, Rahim NA, VanderWaal KE, Gertler FB, Lanier LM (2004). Arp2/3 is a negative regulator of growth cone translocation. Neuron 43, 81–94.
Svitkina TM, Bulanova EA, Chaga OY, Vignjevic DM, Kojima S, Vasiliev JM, Borisy GG (2003). Mechanism of filopodia initiation by reorganization of a dendritic network. J Cell Biol 160, 409–421.
Tamkun JW, DeSimone DW, Fonda D, Patel RS, Buck C, Horwitz AF, Hynes RO (1986). Structure of integrin, a glycoprotein involved in the transmembrane linkage between fibronectin and actin. Cell 46, 271–282.
Wallar BJ, Alberts AS (2003). The formins: active scaffolds that remodel the cytoskeleton. Trends Cell Biol 13, 435–446.
Wallar BJ, Stropich BN, Schoenherr JA, Holman HA, Kitchen SM, Alberts AS (2006). The basic region of the diaphanous-autoregulatory domain (DAD) is required for autoregulatory interactions with the diaphanous-related formin inhibitory domain. J Biol Chem 281, 4300–4307.
Watanabe N, Kato T, Fujita A, Ishizaki T, Narumiya S (1999). Cooperation between mDia1 and ROCK in Rho-induced actin reorganization. Nat Cell Biol 1, 136–143.
Wen Y, Eng CH, Schmoranzer J, Cabrera-Poch N, Morris EJ, Chen M, Wallar BJ, Alberts AS, Gundersen GG (2004). EB1 and APC bind to mDia to stabilize microtubules downstream of Rho and promote cell migration. Nat Cell Biol 6, 820–830.
Williamson T, Gordon-Weeks PR, Schachner M, Taylor J (1996). Microtubule reorganization is obligatory for growth cone turning. Proc Natl Acad Sci USA 93, 15221–15226.
Winkelman JD, Bilancia CG, Peifer M, Kovar DR (2014). Ena/VASP Enabled is a highly processive actin polymerase tailored to self-assemble parallel-bundled F-actin networks with fascin. Proc Natl Acad Sci USA 111, 4121–4126.
Wu D-Y, Goldberg DJ (1993). Regulated tyrosine phosphorylation at the tips of growth cone filopodia. J Cell Biol 123, 653–664.
Yang C, Czech L, Gerboth S, Kojima S, Scita G, Svitkina T (2007). Novel roles of formin mDia2 in lamellipodia and filopodia formation in motile cells. PLoS Biol 5, e317.
Zaidel-Bar R, Ballestrem C, Kam Z, Geiger B (2003). Early molecular events in the assembly of matrix adhesions at the leading edge of migrating cells. J Cell Sci 116, 4605–4613.
Zigmond SH, Evangelista M, Boone C, Yang C, Dar AC, Sicheri F, Forkey J, Pring M (2003). Formin leaky cap allows elongation in the presence of tight capping proteins. Curr Biol 13, 1820–1823.